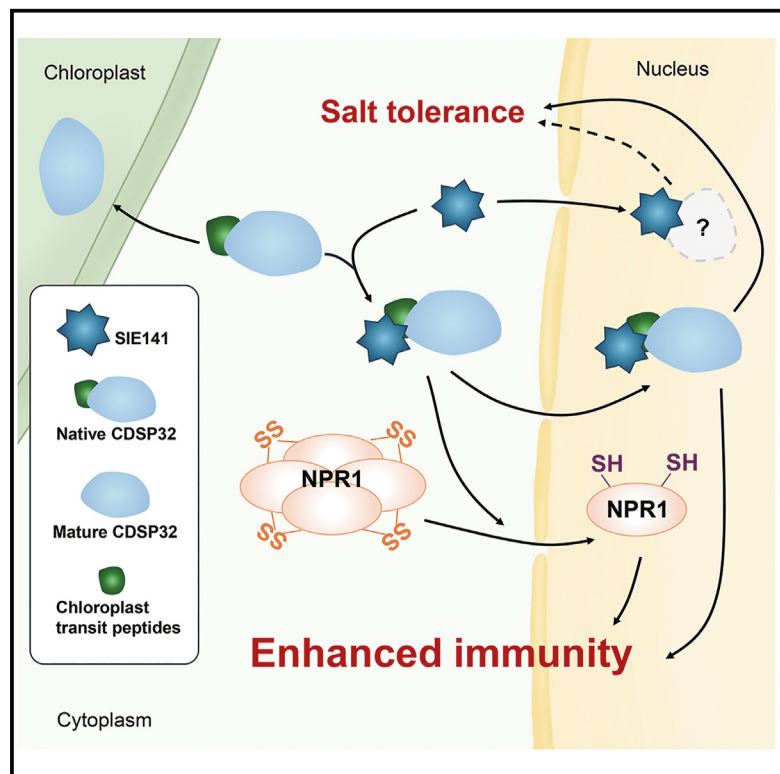


A symbiont fungal effector relocalizes a plastidic oxidoreductase to nuclei to induce resistance to pathogens and salt stress

Graphical abstract



Authors

Yingqi Zhang, Ziran Yang,
Yang Yang, ..., Yuling Meng,
Patrick Schäfer, Weixing Shan

Correspondence

wxshan@nwafu.edu.cn

In brief

Zhang et al. find that effector SIE141 mediates beneficial fungus-induced plant resistance diversity by targeting the plastid protein CDSP32 into host nucleus, enhancing its oxidoreductase activity and ability to monomerize NPR1. Nuclear targeting enables CDSP32 to enhance plant resistance to biotic *Phytophthora* and abiotic salt stresses.

Highlights

- Symbiotic *Serendipita indica* effector SIE141 mediates plant resistance diversity
- SIE141 targets thioredoxin-like CDSP32 and enables it to depolymerize NPR1
- SIE141 binding targets plastid CDSP32 into plant nucleus
- Nuclear-localized CDSP32 enhances plant resistance to biotic and abiotic stresses



Article

A symbiont fungal effector relocalizes a plastidic oxidoreductase to nuclei to induce resistance to pathogens and salt stress

Yingqi Zhang,¹ Ziran Yang,¹ Yang Yang,^{1,3} Aiping Han,¹ Laura Rehneke,² Liwen Ding,¹ Yushu Wei,¹ Zeming Liu,¹ Yuling Meng,¹ Patrick Schäfer,² and Weixing Shan^{1,3,4,*}

¹State Key Laboratory for Crop Stress Resistance and High-Efficiency Production and College of Agronomy, Northwest A&F University, Yangling, Shaanxi 712100, China

²Institute of Phytopathology, Land Use and Nutrition, Research Centre for BioSystems, Justus Liebig University, 35392 Giessen, Germany

³State Key Laboratory for Crop Stress Resistance and High-Efficiency Production and College of Plant Protection, Northwest A&F University, Yangling, Shaanxi 712100, China

⁴Lead contact

*Correspondence: wxshan@nwafu.edu.cn

<https://doi.org/10.1016/j.cub.2024.05.064>

SUMMARY

The root endophytic fungus *Serendipita indica* establishes beneficial symbioses with a broad spectrum of plants and enhances host resilience against biotic and abiotic stresses. However, little is known about the mechanisms underlying *S. indica*-mediated plant protection. Here, we report *S. indica* effector (SIE) 141 and its host target CDSP32, a conserved thioredoxin-like protein, and underlying mechanisms for enhancing pathogen resistance and abiotic salt tolerance in *Arabidopsis thaliana*. SIE141 binding interfered with canonical targeting of CDSP32 to chloroplasts, leading to its re-location into the plant nucleus. This nuclear translocation is essential for both their interaction and resistance function. Furthermore, SIE141 enhanced oxidoreductase activity of CDSP32, leading to CDSP32-mediated monomerization and activation of NON-EXPRESSOR OF PATHOGENESIS-RELATED 1 (NPR1), a key regulator of systemic resistance. Our findings provide functional insights on how *S. indica* transfers well-known beneficial effects to host plants and indicate CDSP32 as a genetic resource to improve plant resilience to abiotic and biotic stresses.

INTRODUCTION

Beneficial microorganisms are frequently utilized by organic farming systems as bio-fertilizers or bio-fungicides to replace chemical pesticides and fertilizers in conventional farming systems.¹ *Serendipita indica* is a beneficial root endophyte that belongs to the order Sebacinales (Basidiomycota) and was initially isolated from the Indian Thar desert.^{2–4} Similar to other filamentous fungi, *S. indica* releases numerous small secreted proteins (SSPs, <300 amino acids [aa]), called effectors, that specifically interact with and modify plant proteins during host colonization.^{5,6} Putative *S. indica* effectors (SIEs) show some host-specific expression profiles, suggesting that *S. indica* may use distinct effectors for host-specific colonization.⁷ Recently, a systematic analysis of 106 SIEs revealed their targets in *Arabidopsis thaliana* (*A. thaliana*) and identified SIEs in changing plant hormone pathways regulating beneficial plant effects.⁸

Enhanced resilience against biotic and abiotic stresses is among the various benefits *S. indica* transfers to host plants.^{3,9–11} In addition to local root resistance, *S. indica* induces systemic resistance in leaves and protects plants against various families of phytopathogens.^{10–12} Among these, *Phytophthora* species are especially devastating oomycete pathogens^{13,14} that include *P. infestans*, as the causal agent of the Irish potato

famine, the soybean root rot pathogen *P. sojae*, and the species complex *P. parasitica* with an extremely broad host range.¹⁵ The bioprotective potential of *S. indica* encouraged investigation of the role of SIEs in triggering resistance to *Phytophthora* pathogens.

Systemic resistance defines a process in which local microbe attacks result in systemic protection of the whole plant.¹⁶ It involves the accumulation of salicylic acid (SA) to launch the monomerization of NON-EXPRESSOR OF PATHOGENESIS-RELATED 1 (NPR1) as a prerequisite for the activation of defense responses, including the induction of *Pathogenesis-related* (PR) genes. A recent study on the crystal structure of NPR1 reveals that it is a bird-shaped homodimer.¹⁷ The unique zinc-finger motif in the BTB domain of NPR1 mediates its oligomerization.¹⁷ Additionally, NPR1 interacts with multiple transcription factors (TFs) as a transcriptional cofactor.¹⁸

Inactive NPR1 forms oligomers based on disulfide bridges. Some thioredoxins participate in the NPR1 monomerization. At least 17 types of thioredoxins and thioredoxin-like proteins were identified in *A. thaliana*.¹⁹ These proteins have oxidoreductase activity and are involved in the regulation of cell redox states.²⁰ Two cysteinyl residues in the conserved catalytic site WC[G/P]PC at the C terminus function in the reduction of disulfide bonds.²⁰ The thioredoxin-like protein CDSP32 was recently identified as a positive regulator of plant non-host resistance and



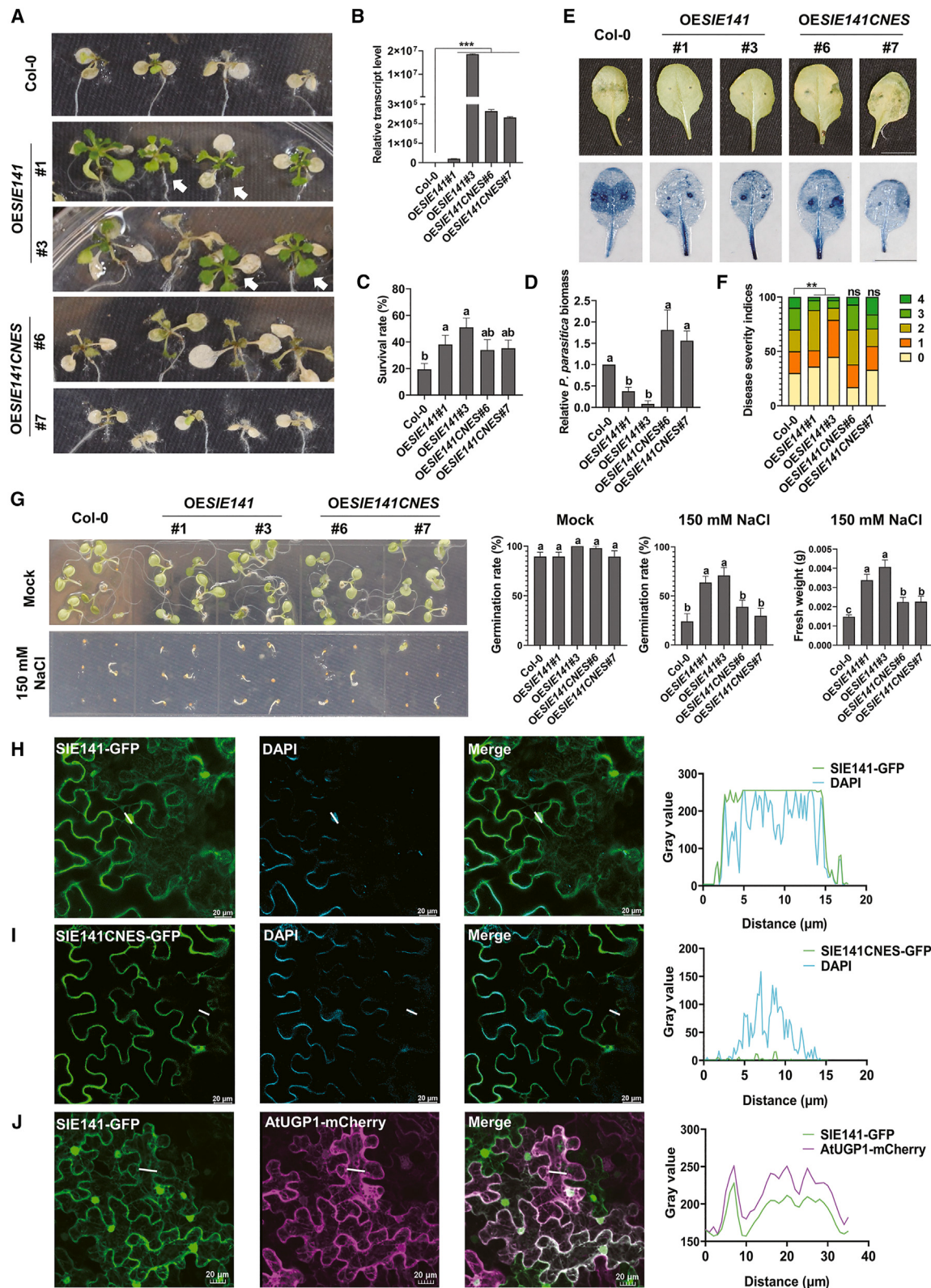


Figure 1. SIE141 is nuclear localized and triggers plant resistance to *Phytophthora parasitica* and salt stress

(A–D) Expression of *SIE141*, but not *SIE141CNES* (with nuclear exclusion signal at C terminus), enhanced *A. thaliana* root immunity to *P. parasitica* (A). RT-qPCR assay to quantify relative *SIE141* transcript levels ($n = 3$) (Student's t test) (B). Infected roots expressing *SIE141* showed an increased survival rate ($n > 10$, one-way

(legend continued on next page)

thermotolerance.²¹ In terms of systemic acquired resistance (SAR), h-type thioredoxins TRXh3 (ATH3) and TRXh5 (ATH5) interact with and monomerize NPR1.¹⁶

In this study, we report on the immune function of SIE141 that we previously found to affect SA signaling in *Arabidopsis thaliana*.⁸ We show that SIE141 specifically targeted CDSP32 and promoted its oxidoreductase activity. SIE141-binding interfered with the chloroplast-transit peptide (CTP) function of CDSP32 and rendered it relocated to the nucleus. We observed an accumulation of chloroplasts around nuclei in SIE141-expressing cells. Furthermore, nuclear-localized CDSP32 led to enhanced disease resistance and salt tolerance, comparable to the levels observed in SIE141-overexpression (OE) gain-of-function transformants. The nuclear translocation was essential for both their interaction and plant resilience function. SIE141-triggered resistance activation was CDSP32-dependent and accompanied by SA accumulation in the roots. Meanwhile, SIE141-binding enhanced CDSP32 oxidoreductase activity and enabled CDSP32-mediated monomerization and activation of NPR1, which subsequently contributes to systemic resistance. These results suggest a mechanistic model in which the beneficial endophytic fungus *S. indica* triggered plant resilience to both biotic and abiotic stresses that critically depends on re-localization of CDSP32 into plant nuclei.

RESULTS

SIE141 endows plants with *P. parasitica* resistance and salt tolerance

Our systematic analysis of 106 SIEs identified SIE141 (PIIN_10643) as an effector that changes SA signaling.⁸ SIE141 is a secreted protein with 198 aa and contains a predicted 18 aa signal peptide at the N terminus, a nuclear-localization signal at residues 74–85 (NLStradamus, posterior = 0.6), and repeated domains at residues 110–130 and 178–198 (GenBank: CAFZ01000892.1). The predicted secretion of the effector was confirmed in a signal peptide assay^{22,23} (Figure S1A). GFP-fused recombinant SIE141 protein was prepared and directly applied to *A. thaliana* seedling roots or infiltrated into *N. benthamiana* leaves to examine its cell entry. DAPI (4',6-diamidino-2-phenylindole) staining and confocal microscopy observation showed that the intensity peaks of green fluorescence merged with DAPI signals overlapped in nuclei (Figures S1B and S1C), indicating cell uptake of SIE141. Plasmolysis of leaf cells confirmed intercellular localization of SIE141 and cell viability (Figure S1C).

The effect of SIE141 on SA suggested a function in plant immunity. We prepared two independent OE lines in *A. thaliana* with substantial SIE141 transcript levels (Figures 1A and 1B). All transformants showed normal growth phenotypes compared with wild-type Col-0 (Figure S1D), except for reduced lateral root density (Figure S1E). Infection assays with *P. parasitica* zoospores showed that the survival rates of OESIE141 seedlings were significantly higher compared with Col-0 at 10 days post inoculation (dpi) (Figures 1A and 1C). Consistently, less *P. parasitica* biomass was detected in infected SIE141 transformants (Figure 1D), indicating that SIE141 OE enhanced root resistance to *P. parasitica*. Infection assays in detached leaves demonstrated decreased disease severity in SIE141-transformants compared with Col-0 at 48 h-post inoculation (hpi) (Figures 1E and 1F), indicating that SIE141 also enhanced *P. parasitica* resistance in *A. thaliana* leaves.

To test if the immune role of SIE141 is conserved across a distant plant species, we transiently expressed SIE141-FLAG and FLAG-GFP in *N. benthamiana* via agroinfiltration, followed by inoculation with *P. infestans* and *P. parasitica* zoospores on detached leaves. The results showed that SIE141 expression limited pathogen infection (Figures S1F and S1G). The expression and integrity of SIE141-FLAG and FGFP were confirmed by western blot (Figure S1H). We further tested the immune function of SIE141 against the necrotrophic pathogens *Rhizoctonia solani* and *Botrytis cinerea* that are sensitive to JA but not SA-triggered immunity. No significant disease resistance was observed in SIE141-transformants compared with Col-0 (Figure S1I), suggesting that SIE141-triggered immunity is not active against necrotrophic pathogens.

Since *S. indica* enhances biotic and abiotic stress resilience in different host plants, we tested SIE141 effects on salt tolerance. SIE141-overexpressing transformants showed higher germination rates and fresh weights, larger leaf areas, and a higher chlorophyll a/b ratio than Col-0 plants after salt treatment (Figures 1G and S1J–S1L), demonstrating that SIE141-expression conferred abiotic stress tolerance in addition to biotic stress resistance.

Nuclear localization of SIE141 is required for triggering plant immunity to Phytophthora pathogens

To identify the subcellular localization of SIE141, we co-expressed SIE141-GFP with cytoplasmic marker AtUGP1-mCherry²⁴ and applied DAPI as nuclear dye in *N. benthamiana* leaves. Confocal microscopy observation showed that SIE141-GFP fluorescence signals overlapped with AtUGP1-mCherry

ANOVA, Brown-Forsythe and Welch test (C) and decreased relative pathogen biomass ($n = 3$, one-way ANOVA, Fisher's LSD test) (D). Arrows indicate surviving seedlings. Lowercase letters indicate statistical significance between multiple groups by one-way ANOVA at $p < 0.05$.

(E) Expression of SIE141, but not SIE141CNES (nuclear-localization mutant), triggered *A. thaliana* leaf immunity to *P. parasitica*. Scale bars, 1 cm.

(F) Infected leaves expressing SIE141 showed decreased disease severity. Disease degrees: 0, no infection; 1, slight infection; 2, mild infection; 3, moderate infection; and 4, severe infection (Mann-Whitney-Wilcoxon test). ** $p \leq 0.01$, ns, no significant differences.

(G) SIE141, but not SIE141CNES, positively regulates plant salt tolerance. Representative images of SIE141-overexpression and SIE141CNES-overexpression lines at 6 days ($n > 8$) post sown on normal growth medium with or without 150 mM NaCl. *A. thaliana* lines overexpressing SIE141 but not SIE141CNES remained significant increase in salt tolerance, as indicated by germination rate. Fresh weight was measured at 10 days after germination under 150 mM NaCl treatment. Statistical analysis was performed with one-way ANOVA (Brown-Forsythe and Welch test). Lowercase letters indicate statistical significance between multiple groups at $p < 0.05$. Error bars give the standard error of mean in graphs (B), (C), (D), and (G).

(H–J) SIE141 localization in the nucleus and cytosol. DAPI staining of *N. benthamiana* leaves transiently expressed SIE141-GFP (H) and SIE141CNES-GFP (I). The SIE141-GFP signal merged with that of cytoplasmic AtUGP1-mCherry (J). The gray value plots show the relative fluorescence along the line in the images. Scale bars, 20 μ m.

See also Figure S1.

and DAPI signals, indicating nuclear and cytoplasmic accumulation of SIE141 (Figures 1H, 1J, S1M, and S1P).

To examine whether nuclear localization is required for SIE141-mediated plant immune activation, we created SIE141 mutants deficient in nuclear localization, according to NLStradmus prediction, by truncating the nuclear-localization signal or mutating its critical residues (SIE141^{ΔNLS} or SIE141^{67-69AAA}) (Figure S1N). However, neither of them rendered SIE141 absent from the whole nucleus, and subsequently, we fused NES (nuclear-export signal) to the C terminus of SIE141 to form SIE141CNES-GFP mutants (Figures S1N and S1O), which were no longer detectable in the nucleus of plant leaf and root cells (Figures 1I and S1M). SIE141CNES-GFP *A. thaliana* transformants were prepared and challenged with *P. parasitica* zoospores. The growth, development, and susceptibility of SIE141CNES-overexpressing plants were comparable to Col-0 (Figures 1A-1F and S1D). This was also observed in *N. benthamiana* detached leaf assays (Figures S1F and S1G). Similar results were observed in salt treatment assays, SIE141CNES-OE transformants lost salt tolerance, as indicated by phenotyping germination rates, fresh weights, and leaf areas (Figures 1G, S1J, and S1K).

SIE141 targets CDSP32, a highly conserved thioredoxin-like plant protein

To further analyze the mechanism by which SIE141 functions in plant immunity, we employed a liquid chromatography-tandem mass spectrometry (LC-MS/MS) approach to identify target proteins in host plants. The C-terminal GFP-tagged SIE141 (with 18 aa signal peptide and C-terminal repeat excluded) was transiently expressed in *N. benthamiana* leaves followed by immunoprecipitation (IP). The immuno-purified proteins were then analyzed by LC-MS/MS, which led to the identification of the 32 kDa thioredoxin-like protein NbCDSP32 (Niben101Scf00539_764277-768892) (Table S1). Its interaction with SIE141 was confirmed by split luciferase and yeast two-hybrid assays (Figures 2A and 2B). CDSP32 is highly conserved across different plant families (Figure S2A; Table S2), and co-immunoprecipitation (coIP) assays with NbCDSP32, AtCDSP32 (AT1G76080), and the *Solanum tuberosum* ortholog StCDSP32 (NCBI: #JX576287) confirmed that SIE141 interacted with all of them (Figure 2C). NbPsbr (Niben101Scf01116g01004.1), a photosystem II 10 kDa polypeptide, was used as the negative control for the yeast two-hybrid assay, while ATHM2 (AT4G03520), an m-type thioredoxin, was used as the negative control for coIP assay. Since the nuclear localization of SIE141 is required for its immune function (Figures 1A-1F and S1F-S1H), we further tested the interaction of AtCDSP32, NbCDSP32, and StCDSP32 with SIE141 nuclear-localization mutants (SIE141CNES-GFP) via coIP assay. These analyses revealed that SIE141CNES strongly reduced its interaction with NbCDSP32 and StCDSP32 (Figure 2D). This failure in interaction was not readily apparent in the case of AtCDSP32, which could potentially be attributed to a higher abundance of AtCDSP32 in the input fraction (Figure 2D). Unlike SIE141CNES, neither SIE141^{67-69AAA} nor SIE141^{ΔNLS} revealed elimination in interactions with CDSP32s (Figure 2D).

Furthermore, we examined the expression profile of AtCDSP32 in Col-0 and SIE141-OE transformants during *P. parasitica* infection. In Col-0 leaves, AtCDSP32 was generally

not induced (Figure S2B), while in Col-0 roots, the expression peaked at 3 hpi before returning to a basic level. In SIE141-OE lines, AtCDSP32 was upregulated at all time points in leaves, while its expression especially increased at 24 hpi in roots (Figure S2B).

Blast search against the TAIR database resulted in 42 thioredoxins that share high sequence similarities with AtCDSP32 protein sequence in *A. thaliana*. These thioredoxins could be classified into 8 types.¹⁹ Most of them neither showed obvious transcriptional changes between SIE141-transformants and Col-0 nor between 0 hpi or 12 hpi with *P. parasitica* (Figure S2C; Table S3). Furthermore, a representative set of the thioredoxins did not interact with SIE141 (Figure S2D), suggesting specific SIE141 targeting of CDSP32.

SIE141-binding mediates nuclear localization of CDSP32

To investigate the co-localization of SIE141 and CDSP32, SIE141-GFP was co-expressed with AtCDSP32-mCherry or NbCDSP32-mCherry, respectively. Confocal microscopy indicated that CDSP32 co-localized with SIE141 at the nucleus (Figures S2E and S2F). We further performed transient co-expression of AtCDSP32-GFP, NbCDSP32-GFP, and StCDSP32-GFP in *N. benthamiana*, respectively, with SIE141-Flag. PcaAvr3a12-Flag²⁵ was used as the negative control. In addition to chloroplast localization, all three CDSP32 proteins consistently accumulated in nuclei in the presence of SIE141-Flag but not PcaAvr3a12 (Figures 3A, 3B, S3A, and S3B). The corresponding protein expression levels in separated cytoplasmic and nuclear fractions confirmed nuclear accumulation of AtCDSP32, NbCDSP32, and, to a weaker extent, StCDSP32 in the presence of SIE141 (Figures 3C, S3C, and S3D).

Mature CDSP32 lacking the CTP has been reported to localize in the chloroplast stroma.^{26,27} This implied that the cytosol-localized effector SIE141 might target the native (full-length) CDSP32 before CTP is cleaved. Bimolecular fluorescence complementation (BiFC) assays indicated that the SIE141-NbCDSP32 complexes appeared to be localized in the cytosol first as predicted, with Pi23014, a nuclear-localized *P. infestans* effector as the negative control²⁸ (Figure 2E). Immunoblot analyses were subsequently conducted with StCDSP32-4MYC and StCDSP32^{ΔCTP}-4MYC (lacking CTP) to examine the relevance of the CTP in SIE141-CDSP32 interaction in the nucleus or cytoplasm. IP detection was less sensitive for AtCDSP32 and NbCDSP32. The results showed that both mature (smaller band without CTP indicated with triangle in Figure 3D) and native StCDSP32 (larger band with CTP, arrow) could be detected in the cytoplasmic fraction. Only native StCDSP32 could be detected in the nuclear fraction in the presence of SIE141 (see asterisk in Figure 3D). We therefore proposed that SIE141 interacts with CDSP32 before CTP cleavage. In accordance with confocal microscopy results (Figures 3A and S3A), SIE141-bound native CDSP32 was thus localized to and accumulated in the nucleus.

CoIP assays indicated a reduced interaction of SIE141 with CTP-truncated mutant AtCDSP32^{ΔCTP} (Figures 4A and 4B). Respective yeast-two-hybrid assay revealed that SIE141 did not interact with AtCDSP32^{ΔCTP} and NbCDSP32^{ΔCTP} (chloroplast-transit-peptide-truncated CDSP32 mutants) (Figure S4A). This indicated that SIE141 might target the CTP of CDSP32 to

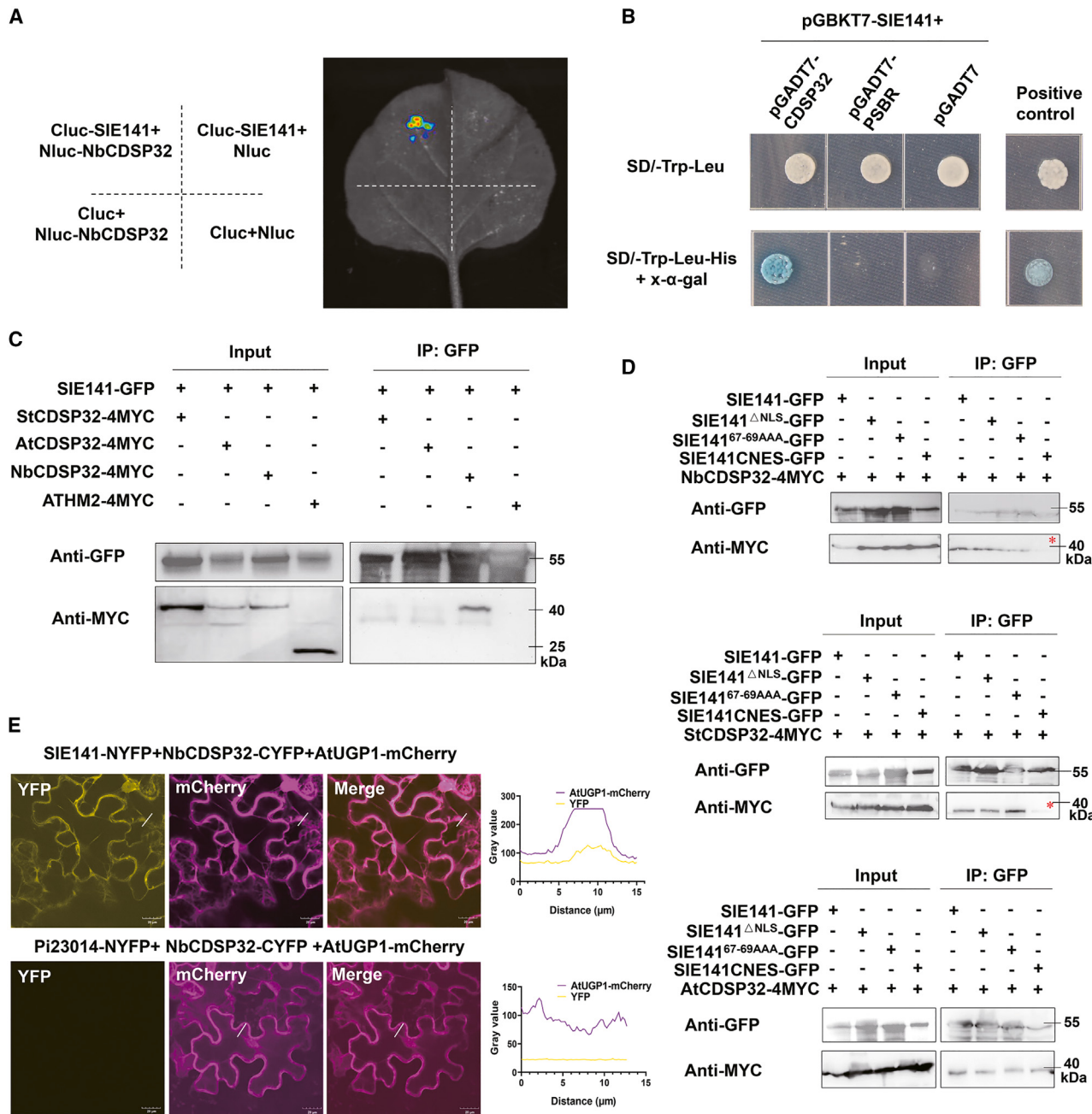


Figure 2. SIE141 specifically interacts with the highly conserved thioredoxin-like protein CDSP32

(A) A luciferase assay to detect interactions between SIE141 and NbCDSP32. *Cluc-SIE141* and *Nluc-NbCDSP32* were co-expressed via agroinfiltration.

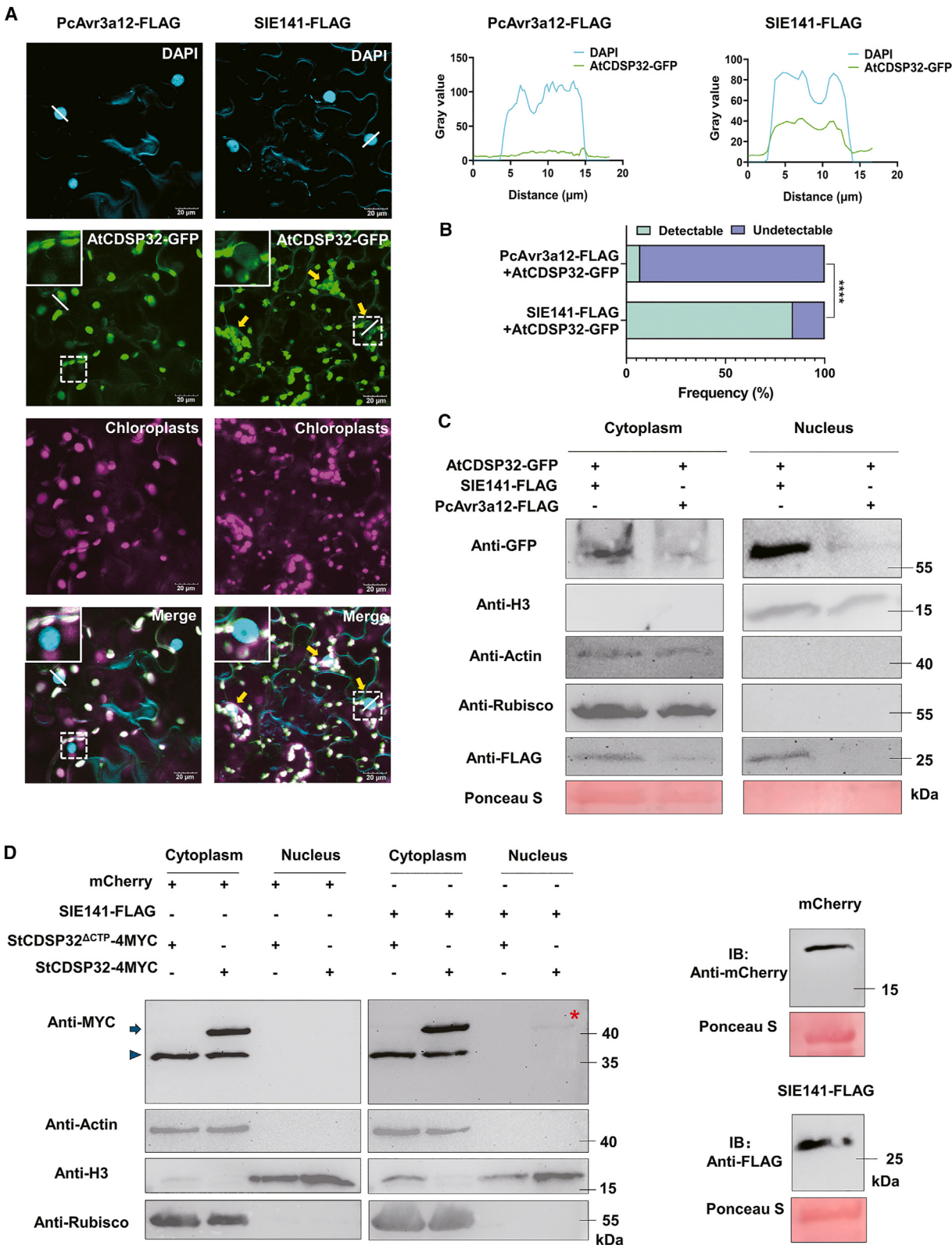
(B) The yeast strain AH109 co-expressing *SIE141* and *NbCDSP32* on SD-/Leu-Trp-His medium showed α -galactosidase activity. AH109 cells co-expressing *SIE141* with *NbPSBR* (a photosystem II 10 kDa polypeptide, the negative control) showed no α -galactosidase activity.

(C) Co-immunoprecipitation (CoIP) assays with GFP-Trap for GFP-fused SIE141, MYC-fused *A. thaliana* AtCDSP32, *N. benthamiana* NbCDSP32, and *Solanum tuberosum* StCDSP32 were detected by the MYC-specific antibody. ATHM2-4MYC (an m-type thioredoxin) was used as the negative control. Protein markers indicate size in kDa.

(D) CoIP assays to detect interactions of NbCDSP32, StCDSP32, and AtCDSP32 with SIE141, mutants SIE141^{ΔNLS} and SIE141^{67-69AAA}, and the nuclear-localization mutant SIE141CNES. Asterisks indicate strongly reduced interactions.

(E) BIFC (bimolecular fluorescence complementation) assay to detect interactions between SIE141 and NbCDSP32 in *N. benthamiana*. C terminus YFP-tagged NbCDSP32 was co-expressed via agroinfiltration with N terminus YFP-tagged SIE141. NbCDSP32-CYFP was co-expressed with Pi23014-NYFP (N terminus of YFP-tagged Pi23014, a nuclear-localized *P. infestans* effector) worked as a negative control. The cytoplasmic AtUGP1-mCherry was co-expressed with SIE141-NYFP+NbCDSP32-CYFP or Pi23014-NYFP+NbCDSP32-CYFP to indicate cytoplasmic localization. The gray value plots show the relative fluorescence along the line in the images. Scale bars, 20 μ m.

See also Figures S1 and S2 and Tables S1 and S3.



interrupt its chloroplast localization. Furthermore, different from NbCDSP32, neither C-terminal NES-fused NbCDSP32 (NbCDS P32CNES) nor NbCDSP32^{ΔCTP} (NbCDSP32^{ΔCTP}CNES) mutant proteins were able to interact with SIE141 (Figure 4C). Taken together, the reduced interaction of the mutant SIE141CNES with CDSP32 (Figure 2D), the nuclear location of SIE141 is crucial for its stable interaction with CDSP32 in the nucleus, and the interaction might be stabilized by the CTP. In addition, the interaction of SIE141 with AtCDSP32^{ΔSGPS}, where the thioredoxin active site (CGPC) of CDSP32 was mutagenized into an inactive site (SGPS, two cysteines changed into two serines), was not abolished (Figure 4B).

CDSP32 positively regulates *P. parasitica* resistance and salt tolerance in *A. thaliana*

To investigate the function of CDSP32 in plant defenses against *Phytophthora* pathogens, we generated *A. thaliana* AtCDSP32-OE and RNA interference (RNAi) knockdown transformants. All of them showed normal plant developments as Col-0 (Figure S5A). The two independent AtCDSP32-OE lines had higher survival rates, less *P. parasitica* colonization, and decreased disease severity, while the AtCDSP32-knockdown lines were as susceptible as Col-0 to *P. parasitica* infection (Figures 4D–4H). No significant differences were detected between either OEAtCDSP32 or RNAiAtCDSP32 transformants and Col-0 in pathogen assays with *B. cinerea* and *R. solani* (Figure S5B). Western blot analyses showed that the mature AtCDSP32 could only be detected in the cytoplasmic fraction but not in the nuclear fraction (Figure S5J).

We also tested resistance mediated by CDSP32s in *N. benthamiana* leaves, with infection assays of *P. parasitica* and *P. infestans*. Regions expressing NbCDSP32 showed significantly smaller lesions compared with FLAG-GFP, as indicated by trypan blue staining (Figures S5C and S5D), suggesting NbCDSP32-promoted plant resistance. Consistent with this, heterologous expression of AtCDSP32 or StCDSP32 also enhanced plant resistance to *Phytophthora* (Figures S5C and S5D). Expression and integrity of fusion proteins were confirmed via western blot (Figure S5E).

A virus-induced gene silencing (VIGS) assay was conducted to knockdown NbCDSP32 in *N. benthamiana* plants (Figure S5F). CDSP32-silencing (*TRV-CDSP32*) did not affect *N. benthamiana* development but resulted in chlorotic leaf spots as previously reported²¹ (Figure S5G). The lesion diameters of detached leaves from *TRV-CDSP32* plants were larger than *TRV-GFP* plants

infected with *P. parasitica* and *P. infestans*, and less pathogen colonization was detected in *TRV-GFP* than in *TRV-CDSP32* leaves (Figures S5H and S5I).

Since SIE141 enhanced salt tolerance in *A. thaliana*, we conducted such assays with CDSP32-OE plants. CDSP32 also enhanced salt tolerance in *A. thaliana*, as demonstrated by higher germination rates and fresh weights, larger leaf areas, and higher chlorophyll contents (except for line OEAtCDSP#3) of the OE transformants (Figures 4I and S5K–S5M). In contrast, lower germination rates and fresh weights were observed in the CDSP32-knockdown plants under salt stress (Figure 4I). Taken together, our analyses showed that CDSP32 positively regulated plant resilience to both biotic *Phytophthora* pathogens and abiotic salt stress.

Nuclear localization and oxidoreductase activity are important for CDSP32-mediated immune activation

A shift to nuclear localization was observed in plant cells expressing AtCDSP32^{ΔCTP}-GFP (Figure 5A). We thus wondered whether nuclear localization and enzymatic activity of CDSP32 directly affected its immune function. We therefore generated *A. thaliana* lines overexpressing AtCDSP32^{ΔCTP} or AtCDSP32^{ΔSGPS}. Infection assays with *P. parasitica* showed reduced pathogen colonization and higher survival rates for AtCDSP32^{ΔCTP}-overexpressing transformants compared with Col-0 (Figures 5B–5D). In contrast, the OEAtCDSP32^{ΔSGPS} lines showed *P. parasitica* biomass and survival rates comparable to Col-0 (Figures 5B–5D). These results indicated that both the nuclear localization and oxidoreductase activity of CDSP32 are important for its immune function. Salt tolerance assays showed that OE of both AtCDSP32^{ΔCTP} and AtCDSP32^{ΔSGPS} increased *A. thaliana* salt tolerance (Figures 4I and S5K–S5M).

Furthermore, OE of NbCDSP32CNLS (C terminus fused nuclear-localization signal) in *N. benthamiana* led to increased immunity to *P. parasitica*, while OE of NbCDSP32CNES (C terminus fused nuclear-export signal) made plants susceptible to the control FGFP expression (Figure S4B). The corresponding protein expression levels in separated cytoplasmic and nuclear fractions were confirmed by western blots (Figure S4C).

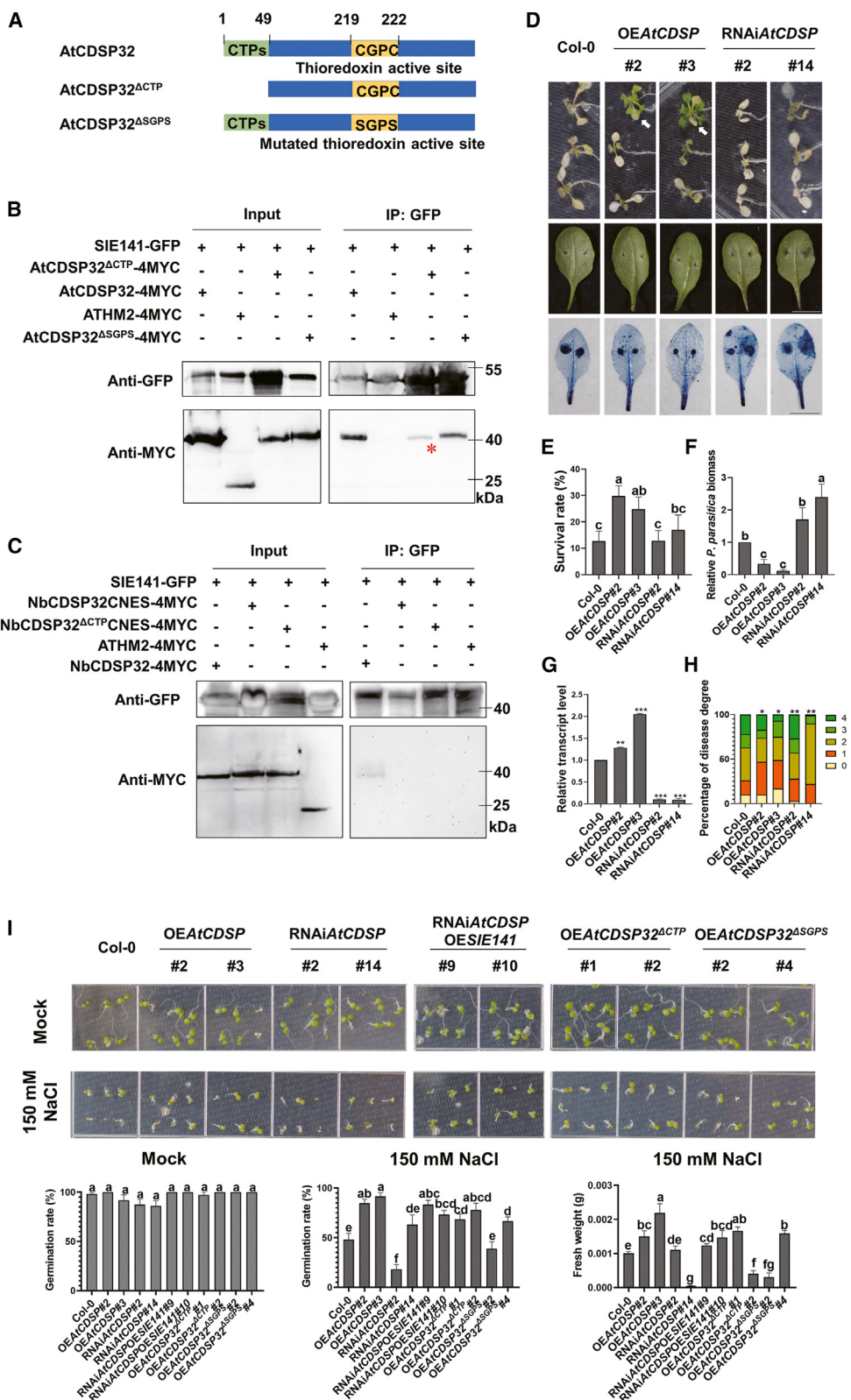
CDSP32 is required for SIE141-mediated resistance to *P. parasitica*

SIE141 relocates native CDSP32 to the nucleus (Figure 3)—we therefore asked if SIE141-activated immunity is relevant

Figure 3. SIE141-binding mediates nuclear localization of CDSP32

- (A) SIE141-FLAG, but not the negative control PcAvr3a12-FLAG, relocates GFP-fused AtCDSP32 into nucleus. DAPI staining was used to visualize the nucleus. Yellow arrows indicate nuclear-localized CDSP32. The gray value plots show the relative fluorescence along the line in the images. Enlarged images of dash boxes were placed at the left-top of GFP or Merge channel images. Scale bars, 20 μm.
- (B) Quantification of the frequency of nuclear CDSP32. “Detectable” indicates the GFP signal observed in the nucleus; “undetectable” indicates no GFP signal detected in the nucleus. $n \geq 80$ individual cells per group. ***, $p = 0.0001$ (Fisher’s exact test).
- (C) Immunoblot analysis for the abundance of AtCDSP32, SIE141-FLAG, and PcAvr3a12-FLAG in nuclear and cytoplasmic extracts from *N. benthamiana* leaf samples that were subjected to confocal microscopy observation in (A). Histone H3, actin, and rubisco were used as controls for the nuclear and cytoplasmic fractions.
- (D) Both mature and native StCDSP32 were detected in the cytoplasm fraction, whereas only native StCDSP32 was detected in the nuclear fraction under SIE141 presence. Immunoblot analysis for StCDSP32-4MYC and StCDSP32^{ΔCTP}-4MYC abundance in nuclear and cytoplasmic extracts from *N. benthamiana* leaves. Mature StCDSP32 (without chloroplast-transit peptide) was marked with triangles, while native StCDSP32 (with chloroplast-transit peptide) was marked with arrows. Native StCDSP32 detected in the nuclear fraction under SIE141 presence was marked with an asterisk. Immunoblot analyses to detect mCherry and SIE141-FLAG with mCherry and FLAG antibodies, respectively.

See also Figure S3.



(legend on next page)

to CDSP32. Two independent *A. thaliana* transformant lines that overexpressed *SIE141* in the *AtCDSP32*-knockdown background (RNAi_i*AtCDSPOESIE141#9* and RNAi_i*AtCDSPOESIE141#10*) showed similar survival rates as *CDSP32*-knockdown seedlings (RNAi_i*AtCDSP#14*) but had lower survival rates than *SIE141* transformants (OES/*SIE141#3*) as well as higher infected root ratios and *P. parasitica* biomass compared with *SIE141*-transformants (Figures S6A–S6D). We also transiently overexpressed *SIE141* and *FGFP* (control) in *TRV-NbCDSP32* and *TRV-GFP N. benthamiana* plants followed by *P. parasitica* or *P. infestans* infection. The results were consistent with those in *A. thaliana* (Figures S6E and S6F).

Although *SIE141* and *CDSP32* activate plant salt tolerance, respectively (Figures 1G and 4I), RNAi_i*AtCDSPOESIE141#9* and RNAi_i*AtCDSPOESIE141#10* lines showed higher germination rates than Col-0 and *CDSP32* knockdown line RNAi_i*AtCDSP#2* under salt stress (Figure 4I). RNAi_i*AtCDSPOESIE141#9* showed significantly higher leaf area, fresh weight, and chlorophyll a/b ratio as compared with Col-0 (Figures S5K–S5M), suggesting that *SIE141*-triggered salt tolerance is not entirely dependent on the target protein *CDSP32*. Taken together, these results confirmed that the *SIE141* immune-activation function for *Phytophthora* pathogens, but not the salt tolerance function, was dependent on *CDSP32*.

SIE141 promotes CDSP32 oxidoreductase activity and NPR1 depolymerization

The thioredoxin-like protein *CDSP32* has a predicted function in redox signaling.²⁰ Its conserved CXXC active sites at the C terminus are critical for oxidoreductase activity.^{21,29} To determine whether *SIE141* affected *CDSP32* enzymatic activity, we isolated recombinant At*CDSP32*, Nb*CDSP32*, St*CDSP32*, and *SIE141* from *Escherichia coli* (Figure S6J). The dithiol-disulfide oxidoreductase activity of each purified protein was tested using an insulin assay,³⁰ with *ATH5* serving as the positive control. All three recombinant *CDSP32* proteins had oxidoreductase activity (Figure 6A). Co-incubation of *SIE141* and At*CDSP32*/Nb*CDSP32*/St*CDSP32* for insulin assay tests showed that

SIE141 enhanced *CDSP32* oxidoreductase activities (Figures S6G–S6I). The negative control, PiAvr3a,¹⁴ was unable to enhance the enzymatic activity of any *CDSP32*.

To further investigate a systemic resistance-related function of *SIE141*, we focused on the oxidoreductase activity of the *SIE141* target *CDSP32* in *NPR1* depolymerization. Since *ATH3* and *ATH5* were previously reported to directly target and participate in the monomerization of *NPR1*,¹⁶ we hypothesized that *CDSP32* may play a similar role. CoIP and luciferase-complementation assays confirmed the interaction of *CDSP32* with *NPR1* in both *A. thaliana* and *N. benthamiana* (Figures 6B–6D). However, in contrast to *ATH5*, neither At*CDSP32* nor Nb*CDSP32* showed capability to depolymerize At*NPR1* (Figure 6E). Since *SIE141* promoted the oxidoreductase activity of At*CDSP32* (Figure S6G), we therefore co-incubated At*CDSP32* or *ATH5* with varying concentrations of recombinant *SIE141* before the thioredoxins were mixed with At*NPR1*. At*CDSP32* could reduce At*NPR1* oligomerization in the presence of *SIE141*, and higher concentrations of *SIE141* corresponded to increased production of At*NPR1* monomers (Figure 6E). In turn, *SIE141* alone could not depolymerize At*NPR1* (Figure S6K).

SA was increased in *SIE141*-expressing plants, and *SIE141* affects SA signaling in plants.⁸ Since *SIE141*-triggered plant resistance to the hemibiotrophic pathogens *P. parasitica* and *P. infestans*, we therefore quantified SA content in *SIE141*-transformants and Col-0 plants with high-performance LC (HPLC)-MS/MS. SA contents were higher in the roots but not the leaves of two independent *SIE141*-OE lines compared with Col-0 (Figure S7A).

Next, we employed RNA sequencing and identified 244 upregulated and 214 downregulated genes in *SIE141*-overexpressing *A. thaliana* transformants compared with Col-0 (Tables S4 and S5). Principal component analyses (PCA) of the resulting datasets of each species demonstrated a clear separation of samples, revealing highly transcriptional changes between *SIE141*-OE transformants and Col-0 (Figure S7B). Subsequent gene ontology (GO) enrichment analysis identified 19 upregulated genes

Figure 4. CDSP32 positively regulates plant resistance to *P. parasitica* and salt tolerance, and chloroplast-transit peptide of CDSP32 is required for SIE141 interaction

- (A) Schematic diagrams showing mutations in *CDSP32*.
- (B) CoIP assay to examine interactions of MYC-fused At*CDSP32* mutants with GFP-fused *SIE141*. Mutations in CTP, marked with an asterisk, but not the thioredoxin active sites, attenuated the interaction.
- (C) *SIE141* does not interact with Nb*CDSP32CNES* (C terminus fused nuclear-export signal) and Nb*CDSP32^{ΔCTP}CNES* (chloroplast-transit peptide-truncated mutant with C terminus fused nuclear-export signal). CoIP assay conducted with GFP-Trap for the GFP-fused *SIE141*, no Nb*CDSP32CNES-4MYC* and Nb*CDSP32^{ΔCTP}CNES-4MYC* were detected by MYC-specific antibody. ATHM2, the negative control.
- (D–H) Infection assays on At*CDSP32*-overexpression *A. thaliana* transformant seedlings (D). Survival rates were scored relative to wild-type Col-0 at 5 dpi ($n > 10$, one-way ANOVA, Brown-Forsythe, and Welch test) (E). Enhanced resistance to *P. parasitica* in independent At*CDSP32*-overexpression but not At*CDSP32*-knockdown lines (F). Pathogen biomass was quantified with qPCR at 48 hpi. $n = 3$, one-way ANOVA, Fisher's LSD test. RT-qPCR assay to quantify At*CDSP32* transcripts (G). Data were analyzed with Student's t test. Detached leaf assays revealed enhanced *P. parasitica* resistance in independent At*CDSP32* over-expression but not At*CDSP32*-knockdown lines (H). Lesion development was scored and conducted with Mann-Whitney-Wilcoxon test. Disease degrees: 0, no infection; 1, slight infection; 2, mild infection; 3, moderate infection; and 4, severe infection. Scale bars, 1 cm. * $p \leq 0.05$, ** $p \leq 0.01$, *** $p \leq 0.001$. Lowercase letters indicate statistical significance between multiple groups by one-way ANOVA at $p < 0.05$.
- (I) *CDSP32* positively regulates plant salt tolerance. Representative images of *A. thaliana* seedlings at 6 days post sown on normal growth medium with or without 150 mM NaCl. *A. thaliana* seeds were sown ($n > 4$), and each bio-repeat contains 6 seeds. Overexpression of At*CDSP32* or its chloroplast-transit peptide mutants independently enhanced salt tolerance. Knockdown of At*CDSP32* or overexpression of thioredoxin active-site mutants showed decreased tolerance to salt stress. For two independent *A. thaliana* lines overexpressing *SIE141* with *CDSP32* knockdown, there was a significant increase in salt tolerance. Fresh weight was observed at 10 days after sown under 150 mM NaCl treatment. Lowercase letters indicate statistical analysis significance with one-way ANOVA at $p < 0.05$ (Brown-Forsythe and Welch test). Error bars give the standard error of mean in graphs (E), (F), (G), and (I).

See also Figures S4 and S5.

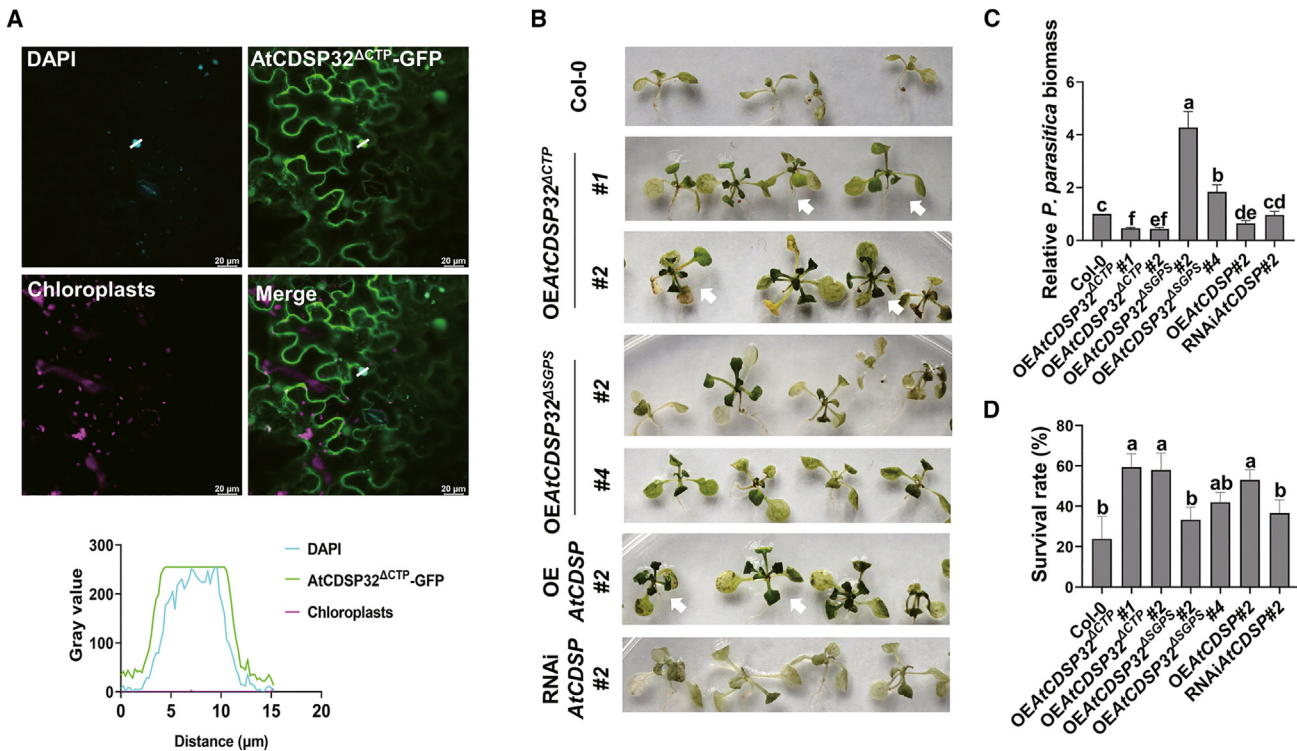


Figure 5. Localization and oxidoreductase activity are crucial for CDSP32 immune function

(A) Co-localization of DAPI with chloroplast-transit peptide-mutated AtCDSP32-GFP. The mutant construct AtCDSP32 Δ CTP-GFP was transiently expressed in *N. benthamiana* via agroinfiltration. Cells were observed at 2 dpi after DAPI staining for 15 min. The graph of gray value shows DAPI, GFP, and chloroplasts fluorescence intensity.

(B–D) Infection assays on 10-day-old *A. thaliana* seedlings revealed enhanced *P. parasitica* resistance in independent chloroplast-transit peptide mutants and enhanced susceptibility in thioredoxin active-site mutants at 5 dpi (B). Quantification of relative pathogen biomass (C) and seedling survival rates after infection with *P. parasitica* (D). Three independent replicates with at least 15 seedlings were tested, one-way ANOVA at $p < 0.05$, Fisher's LSD test. Seedling survival rates were determined at 5 dpi with *P. parasitica* ($n > 10$, one-way ANOVA at $p < 0.05$, Brown-Forsythe and Welch test). Lowercase letters indicate statistical significance tested between multiple groups. Error bars give the standard error of mean.

See also Figure S4.

involved in SAR pathway with some of them directly involved in plant defense responses against oomycete pathogens,^{31,32} e.g., AT2G14560 (*LURP1*, LATE UPREGULATED IN RESPONSE TO HYALOPERONOSPORE PARASITICA1), AT4G10500 (*DLO1*, DMR6-LIKE OXYGENASE1), and AT4G11890 (*ARCK1*, ABA-AND OSMOTIC-STRESS-INDUCIBLE RECEPTOR-LIKE CYTOSOLIC KINASE1) (Figures S7C and S7D). As anticipated, the *NPR1*-dependent gene *PR1*, but not *NPR1* itself, was significantly upregulated in the *SIE141*-OE lines at 0 and 6 hpi with *P. parasitica* inoculation (Figure S7E). *CBP60g*, a TF contributing to SA biosynthesis,³³ was upregulated at 0 hpi in the *SIE141*-transformants. Furthermore, *LURP1* and *ARCK1*, which are related to SAR, were significantly upregulated in *SIE141*-transformants. However, *DLO1*, a suppressor of immunity in *A. thaliana*,³⁴ was downregulated (Figure S7E).

Taken together, the analyses demonstrated that *SIE141* targeted CDSP32 and promoted its oxidoreductase activity resulting in the monomerization of *NPR1*. Additionally, *SIE141*-transformants showed SA accumulation in the roots and upregulation of 19 SAR-related genes. These results suggest that *SIE141*-mediated activation of plant resistance involves *NPR1*-mediated systemic resistance.

DISCUSSION

Sustainable agriculture practices have become increasingly important for biological control approaches and integrated disease management. *S. indica*, a beneficial fungal endophyte, reportedly enhances plant resilience to various biotic and abiotic stresses.³⁵ *S. indica* secretes a series of effectors^{5,7} that have been known to modify the plant immune system and promote fungal colonization.^{36–38}

In this study, we determined the mechanism by which *SIE141* assists in plant immunity against phytopathogens. *SIE141*, which we previously found to affect SA signalling in *Arabidopsis*,⁸ was shown to enhance resistance to *Phytophthora* pathogens (Figure 1) and to enhance the oxidoreductase activity of its target CDSP32, a positive regulator of plant immunity (Figures 2A–2C, 4D–4H, and S6G).

We utilized recombinant GFP-fused *SIE141* protein to determine its cell-entry activity. Recombinant fungal and oomycete effector proteins are well-documented to enter host plant cells, though the underlying cell-entry mechanisms are not very clear. Endocytosis and external PI3P were found to be involved in effector cell entry, while host receptor proteins have not been

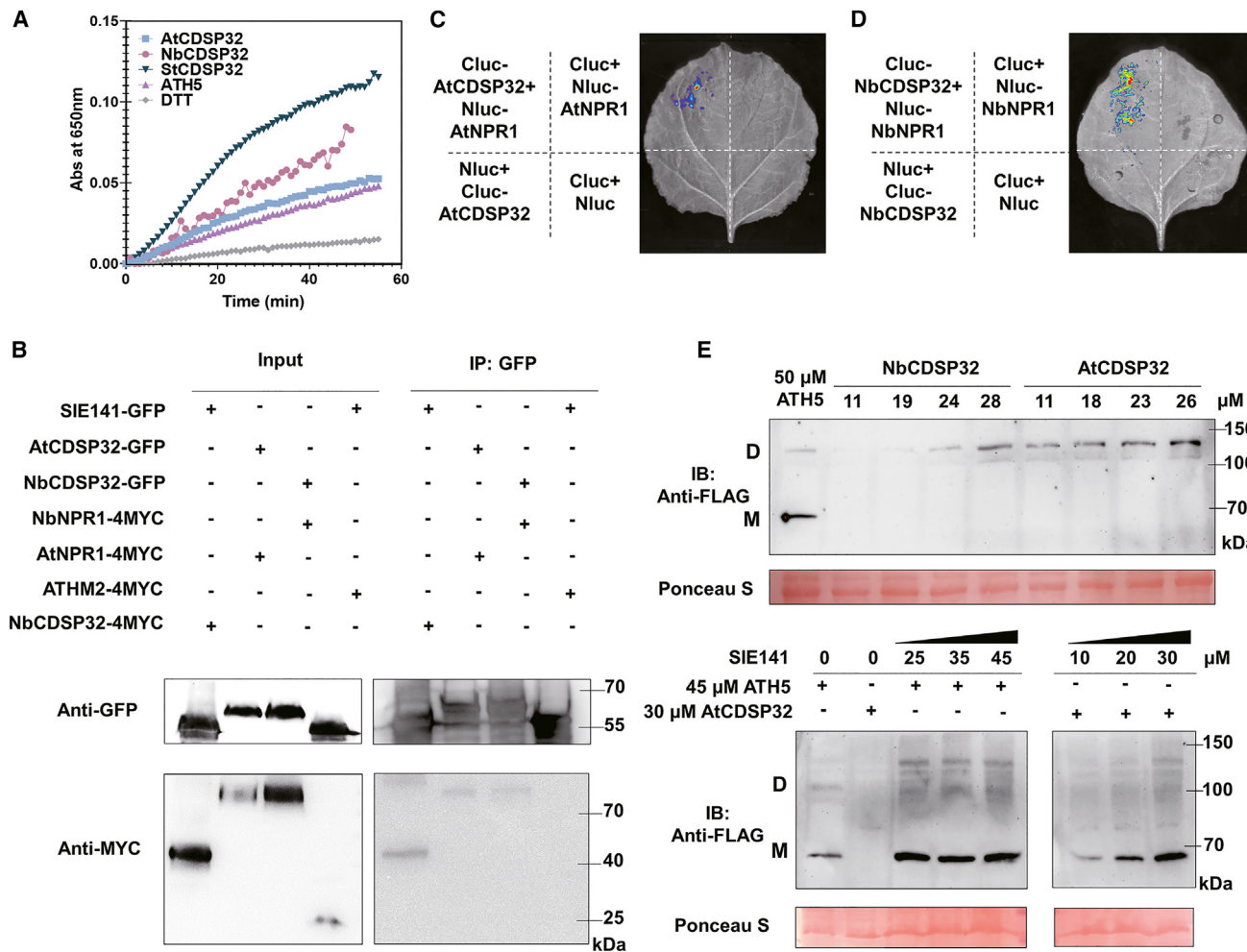


Figure 6. CDSP32 monomerizes NPR1 in a SIE141-dependent manner

(A) Thioredoxin oxidoreductase activities of AtCDSP32, NbCDSP32, and StCDSP32 were measured with insulin as the substrate. Recombinant ATH5 served as a positive control. DTT group served as the negative control.

(B) CDSP32 interacts with NPR1. Proteins were extracted from *N. benthamiana* leaves co-expressing AtCDSP32-GFP+AtNPR1-4MYC or NbCDSP32-GFP+NbNPR1-4MYC using a GFP-Trap. AtCDSP32 and NbCDSP32 were detected with GFP antibody. AtNPR1 and NbNPR1 were detected with MYC antibody. SIE141-GFP+ATHM2-4MYC worked as the negative control, while SIE141-GFP+NbCDSP32-4MYC worked as the positive control.

(C and D) Luciferase-complementation assays to detect interactions between AtNPR1 and AtCDSP32 (C) and NbNPR1 and NbCDSP32 (D). Cluc-AtCDSP32 and Nluc-AtNPR1 or Cluc-NbCDSP32 and Nluc-NbNPR1 were co-expressed, respectively, via agroinfiltration. Luminescence signals were recorded in *N. benthamiana* leaves at 48 hpi.

(E) SIE141 enables a dose-dependent manner of CDSP32 to reduce AtNPR1-FLAG dimer complexes (D) to monomers (M) *in vitro*. Ponceau S was used to verify equal protein loading.

See also Figures S6 and S7.

identified yet.^{39,40} The purified SIE141 was determined to be biologically active as shown in the co-incubation with its target CDSP32 in enhancing oxidoreductase activity. The documented applications of purified GFP-fused effector protein to plant tissues/protoplasts for determining the cell entry of effectors are reported.^{39,41} Therefore, all *A. thaliana* transgenic lines that express individual SIE effectors were based on their intracellular localization/functions.⁸

Our analyses showed that SIE141-NbCDSP32 complex localizes in both the cytosol and nucleus (Figures 2E, S2E, and S2F). CDSP32 is a chloroplast-targeting protein, and SIE141-binding of full-length CDSP32 abolished its chloroplast-targeting function,

which suggests that initial SIE141-CDSP32 complex formation takes place in the cytosol. CDSP32 might carry unknown nuclear-localization signals that lead to the SIE141-CDSP32 complex entering the nucleus. This nuclear localization is crucial for the observed resistance phenotype, as evidenced by the enhanced immunity of plants overexpressing NbCDSP32CNLS (Figure S4B). However, since both chloroplast-targeting and nuclear localization of CDSP32 are important for enhanced disease resistance, its forced expression in the cytoplasm by fusion with a nuclear-export signal (NES) successfully abolished its nuclear localization and significantly decreased its chloroplast-targeting (Figure S4C), leading to plant susceptibility (Figure S4B).

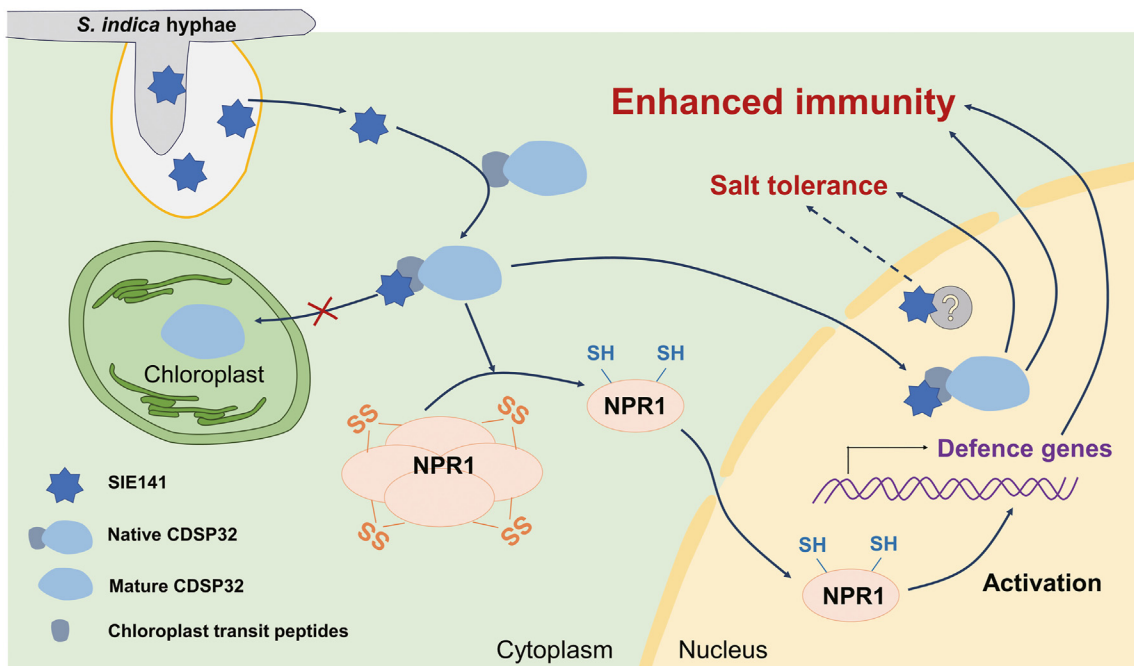


Figure 7. Schematic model for the *S. indica* effector SIE141-triggered plant resistance to pathogens and salt stress

SIE141 interrupts chloroplast-transit peptide function of CDSP32. SIE141-binding of the full-length CDSP32 in the cytosol abolishes its chloroplast-targeting and leads to re-localization to the host nucleus. SIE141 also enables CDSP32 in the cytosol to depolymerize NPR1 and promotes NPR1-dependent defense responses. Nuclear-localized SIE141 and CDSP32 trigger enhanced plant resistance to *Phytophthora* pathogens. CDSP32 and SIE141 independently trigger enhanced salt tolerance, and SIE141 might bind unknown target(s) (the question mark) through unknown mechanisms (dotted lines) to enhance salt tolerance.

On the other hand, CDSP32 directly interacted with NPR1, and SIE141-binding rendered CDSP32-mediated NPR1 depolymerization, a critical step for its immune function. This is highly interesting, as *S. indica* was known to depend on NPR1 for its ability to activate induced systemic resistance (ISR).⁴² ISR is defined to be activated by root-colonizing plant growth-promoting bacteria/fungi and, in contrast to SAR, was always thought to act independently of SA. Recent reports, however, suggest a less clear separation of ISR and SAR signaling.⁴³ Consistent with this, NPR1 is known to participate in both ISR and SAR.⁴⁴ This study revealed SIE141 as a potentially helpful tool to provide more details about the regulation of systemic resistance in plants. In this respect, it will be interesting to uncover in the future if the observed nuclear SIE141-CDSP32 interaction triggers nuclear entry of NPR1 and its function as a transcriptional co-regulator of systemic resistance mediated by *S. indica*.¹⁷

SA stabilizes NPR1, while SA signals are known to repress LR development.⁴⁵ The observed reduced LR density in SIE141 transformants might be the result of SA accumulation in SIE141-transformant roots (Figure S1E). Because LRs are potential pathogen entry and colonization sites,⁴⁵ SIE141 could shape plant root morphology via SA accumulation to restrain local root infections.

Both OES/E141 and OECDSP32 lines exhibit physiological and morphological traits that are indicative of enhanced salt tolerance (Figures 1G and 4I). However, *A. thaliana* lines expressing RNAiCDSP32OES/E141 remained salt-tolerant (Figure 4I). This indicated that CDSP32 knockdown was insufficient to block SIE141 function in triggering salt tolerance. On the one

hand, our study revealed that CDSP32 functions as a thioredoxin and thus participates in the redox signaling pathway to regulate ROS homeostasis required for increased salt tolerance.^{46,47} On the other hand, SIE141 most likely has other targets in addition to CDSP32 to regulate different pathways involved in SIE141-mediated functions (Figure 7). For instance, as described in this study (Figure S7A) and a previous report,⁸ SIE141 modulates SA signaling in *A. thaliana*. Since SA interplays with other phytohormones (e.g., auxins, brassinosteroids, ethylene, and abscisic acid) and signaling molecules during salt stress,⁴⁸ SIE141 is more likely to participate in the metabolic network of plant hormones that regulate salt tolerance.

In conclusion, we found that SIE141 triggered plant resistance by interfering with the plastid import of CDSP32, leading to its redirection to the nucleus and monomerization of NPR1 (Figure 7). SIE141 also increased salt tolerance in *A. thaliana*, indicating a direct role of an effector in activating beneficial functions well-known to be mediated by *S. indica*.

STAR METHODS

Detailed methods are provided in the online version of this paper and include the following:

- KEY RESOURCES TABLE
- RESOURCE AVAILABILITY
 - Lead contact
 - Materials availability
 - Data and code availability
- EXPERIMENTAL MODEL AND STUDY PARTICIPANT DETAILS

- Plant growth conditions and surface sterilization steps
- Bacteria, yeasts, *Phytophthora* and fungal pathogens, and their growth conditions
- **METHOD DETAILS**
 - Plasmid construction
 - Pathogen infection assays
 - Transient expression and VIGS assays in *N. benthamiana*
 - Yeast two-hybrid (Y2H) assay
 - Bimolecular fluorescence complementation (BiFC) assay
 - Co-immunoprecipitation assay (co-IP) and western blot assays
 - Functional evaluation of PIN1_10643 signal peptide sequences
 - Recombinant protein purification
 - Thioredoxin activity assay
 - Real-time quantitative PCR (qRT-PCR) and quantitative reverse transcription PCR (RT-qPCR)
 - Reduction of NPR1 oligomers to monomers by thioredoxins
 - Confocal microscopy
 - SA measurements with HPLC-MS/MS
 - Luciferase assay
 - RNA sequencing and transcriptome analysis
 - Salt stress treatment and analysis
 - Cytoplasm and nuclear fraction separation and protein extraction
 - Phylogenetic tree construction for orthologs of CDSP32
- **QUANTIFICATION AND STATISTICAL ANALYSIS**
 - Image processing and data analysis
 - Statistical analysis

SUPPLEMENTAL INFORMATION

Supplemental information can be found online at <https://doi.org/10.1016/j.cub.2024.05.064>.

ACKNOWLEDGMENTS

We thank Dr. Brett Tyler for suggestions; Dr. Xuehong Wu (China Agricultural University) for *Rhizoctonia solani*; and Ms. Yan Li (College of Plant Protection, Northwest A&F University) and Ms. Zhenzhen Ma (CBIC, College of Agronomy, Northwest A&F University), Ms. Meijuan Ren (LSRCS, Northwest A&F University), and Ms. Liru Jian (SKLCSRHEP, Northwest A&F University) for technical support in confocal microscopy, LC-MS/MS, and HPLC-MS/MS, respectively. This work was supported by the Strategic Priority Research Program of the Chinese Academy of Sciences (no. XDA23070201), the Agricultural Breeding Program from the Ningxia Department of Science and Technology (2019NYYZ01), the China Agriculture Research System (#CARS-09), and the State Administration for Foreign Experts Affairs (#B18042).

AUTHOR CONTRIBUTIONS

Conceptualization, W.S., Y.Z., and P.S.; investigation, Y.Z., Z.Y., and A.H.; methodology, Y.Z. and Y.Y.; software, Y.W.; formal analysis, Y.Z.; resources, P.S. and L.R.; writing—original draft, Y.Z.; writing—review & editing, W.S. and P.S.; funding acquisition, W.S. and Y.M.; visualization, Z.Y. and Y.Y.; supervision, W.S. and P.S.

DECLARATION OF INTERESTS

A patent based on this study has been filed by Northwest A&F University with W.S., Y.Z., and Y.M. as inventors.

Received: January 12, 2024

Revised: April 24, 2024

Accepted: May 29, 2024

Published: June 24, 2024

REFERENCES

1. Xia, Y., Sahib, M.R., Amna, A., Opiyo, S.O., Zhao, Z., and Gao, Y.G. (2019). Culturable endophytic fungal communities associated with plants in organic and conventional farming systems and their effects on plant growth. *Sci. Rep.* 9, 1669. <https://doi.org/10.1038/s41598-018-38230-x>.
2. Varma, A., Savita, V., Sudha, Sahay, N., Butehorn, B., and Franken, P. (1999). *Piriformospora indica*, a cultivable plant-growth-promoting root endophyte. *Appl. Environ. Microbiol.* 65, 2741–2744. <https://doi.org/10.1128/AEM.65.6.2741-2744.1999>.
3. Baltruschat, H., Fodor, J., Harrach, B.D., Niemczyk, E., Barna, B., Gullner, G., Janeckzo, A., Kogel, K.H., Schäfer, P., Schwarzcinger, I., et al. (2008). Salt tolerance of barley induced by the root endophyte *Piriformospora indica* is associated with a strong increase in antioxidants. *New Phytol.* 180, 501–510. <https://doi.org/10.1111/j.1469-8137.2008.02583.x>.
4. Weiβ, M., Waller, F., Zuccaro, A., and Selosse, M.A. (2016). Sebacinales – one thousand and one interactions with land plants. *New Phytol.* 211, 20–40. <https://doi.org/10.1111/nph.13977>.
5. Rafiqi, M., Jelonek, L., Akum, N.F., Zhang, F., and Kogel, K.H. (2013). Effector candidates in the secretome of *Piriformospora indica*, a ubiquitous plant-associated fungus. *Front. Plant Sci.* 4, 228. <https://doi.org/10.3389/fpls.2013.00228>.
6. Zuccaro, A., Lahrmann, U., Güldener, U., Langen, G., Pfiffi, S., Biedenkopf, D., Wong, P., Samans, B., Grimm, C., Basiewicz, M., et al. (2011). Endophytic life strategies decoded by genome and transcriptome analyses of the mutualistic root symbiont *Piriformospora indica*. *PLoS Pathog.* 7, e1002290. <https://doi.org/10.1371/journal.ppat.1002290>.
7. Lahrmann, U., Ding, Y., Banbara, A., Rath, M., Hajirezaei, M.R., Döhleman, S., von Wirén, N., Parniske, M., and Zuccaro, A. (2013). Host-related metabolic cues affect colonization strategies of a root endophyte. *Proc. Natl. Acad. Sci. USA* 110, 13965–13970.
8. Osborne, R., Rehneke, L., Lehmann, S., Roberts, J., Altmann, M., Altmann, S., Zhang, Y., Köppf, E., Dominguez-Ferreras, A., Okechukwu, E., et al. (2023). Symbiont-host interactome mapping reveals effector-targeted modulation of hormone networks and activation of growth promotion. *Nat. Commun.* 14, 4065. <https://doi.org/10.1038/s41467-023-39885-5>.
9. Hosseini, F., Mosaddeghi, M.R., and Dexter, A.R. (2017). Effect of the fungus *Piriformospora indica* on physiological characteristics and root morphology of wheat under combined drought and mechanical stresses. *Plant Physiol. Biochem.* 118, 107–120. <https://doi.org/10.1016/j.plaphy.2017.06.005>.
10. Narayan, O.P., Verma, N., Singh, A.K., Oelmüller, R., Kumar, M., Prasad, D., Kapoor, R., Dua, M., and Johri, A.K. (2017). Antioxidant enzymes in chickpea colonized by *Piriformospora indica* participate in defense against the pathogen *Botrytis cinerea*. *Sci. Rep.* 7, 13553. <https://doi.org/10.1038/s41598-017-12944-w>.
11. Nassimi, Z., and Taheri, P. (2017). Endophytic fungus *Piriformospora indica* induced systemic resistance against rice sheath blight via affecting hydrogen peroxide and antioxidants. *Biocontrol Sci. Technol.* 27, 252–267. <https://doi.org/10.1080/09583157.2016.1277690>.
12. Trzewik, A., Maciorowski, R., Klocke, E., and Orlikowska, T. (2020). The influence of *Piriformospora indica* on the resistance of two rhododendron cultivars to *Phytophthora cinnamomi* and *P. plurivora*. *Biol. Control* 140, 104121. <https://doi.org/10.1016/j.biocntrol.2019.104121>.
13. Yang, Y., Zhao, Y., Zhang, Y., Niu, L., Li, W., Lu, W., Li, J., Schäfer, P., Meng, Y., and Shan, W. (2022). A mitochondrial RNA processing protein mediates plant immunity to a broad spectrum of pathogens by modulating the mitochondrial oxidative burst. *Plant Cell* 34, 2343–2363. <https://doi.org/10.1093/plcell/koac082>.
14. Li, T., Wang, Q., Feng, R., Li, L., Ding, L., Fan, G., Li, W., Du, Y., Zhang, M., Huang, G., et al. (2019). Negative regulators of plant immunity derived from cinnamyl alcohol dehydrogenases are targeted by multiple *Phytophthora Avr3a*-like effectors. *New Phytol.* <https://doi.org/10.1111/nph.16139>.
15. Lu, W., Deng, F., Jia, J., Chen, X., Li, J., Wen, Q., Li, T., Meng, Y., and Shan, W. (2020). The *Arabidopsis thaliana* gene *AtERF019* negatively regulates plant resistance to *Phytophthora parasitica* by suppressing PAMP-triggered immunity. *Mol. Plant Pathol.* 21, 1179–1193. <https://doi.org/10.1111/mpp.12971>.

16. Tada, Y., Spoel, S.H., Pajerowska-Mukhtar, K., Mou, Z., Song, J., Wang, C., Zuo, J., and Dong, X. (2008). Plant immunity requires conformational changes of NPR1 via S-nitrosylation and thioredoxins. *Science* 321, 952–956. <https://doi.org/10.1126/science.1156970>.
17. Kumar, S., Zavaliev, R., Wu, Q., Zhou, Y., Cheng, J., Dillard, L., Powers, J., Withers, J., Zhao, J., Guan, Z., et al. (2022). Structural basis of NPR1 in activating plant immunity. *Nature* 605, 561–566. <https://doi.org/10.1038/s41586-022-04699-w>.
18. Zhou, P., Zavaliev, R., Xiang, Y., and Dong, X. (2023). Seeing is believing: Understanding functions of NPR1 and its paralogs in plant immunity through cellular and structural analyses. *Curr. Opin. Plant Biol.* 73, 102352. <https://doi.org/10.1016/j.pbi.2023.102352>.
19. Meyer, Y., Reichheld, J.P., and Vignols, F. (2005). Thioredoxins in *Arabidopsis* and other plants. *Photosynth. Res.* 86, 419–433. <https://doi.org/10.1007/s11120-005-5220-y>.
20. Gelhaye, E., Rouhier, N., Navrot, N., and Jacquot, J.P. (2005). The plant thioredoxin system. *Cell. Mol. Life Sci.* 62, 24–35. <https://doi.org/10.1007/s00018-004-4296-4>.
21. Pant, B.D., Oh, S., Lee, H.K., Nandety, R.S., and Mysore, K.S. (2020). Antagonistic regulation by CPN60A and CLPC1 of TRXL1 that regulates MDH activity leading to plant disease resistance and thermotolerance. *Cell Rep.* 33, 108512. <https://doi.org/10.1016/j.celrep.2020.108512>.
22. Zhang, Q., Li, W., Yang, J., Xu, J., Meng, Y., and Shan, W. (2020). Two *Phytophthora parasitica* cysteine protease genes, *PpCys44* and *PpCys45*, trigger cell death in various *Nicotiana* spp. and act as virulence factors. *Mol. Plant Pathol.* 21, 541–554. <https://doi.org/10.1111/mpp.12915>.
23. Gu, B., Kale, S.D., Wang, Q., Wang, D., Pan, Q., Cao, H., Meng, Y., Kang, Z., Tyler, B.M., and Shan, W. (2011). Rust secreted protein Ps87 is conserved in diverse fungal pathogens and contains a RXLR-like motif sufficient for translocation into plant cells. *PLoS ONE* 6, e27217. <https://doi.org/10.1371/journal.pone.0027217>.
24. Park, J.I., Ishimizu, T., Suwabe, K., Sudo, K., Masuko, H., Hakozaki, H., Nou, I.S., Suzuki, G., and Watanabe, M. (2010). UDP-glucose pyrophosphorylase is rate limiting in vegetative and reproductive phases in *Arabidopsis thaliana*. *Plant Cell Physiol.* 51, 981–996. <https://doi.org/10.1093/pcp/pcq057>.
25. Fan, G., Yang, Y., Li, T., Lu, W., Du, Y., Qiang, X., Wen, Q., and Shan, W. (2018). A *Phytophthora capsici* RXLR effector targets and inhibits a plant PPIase to suppress endoplasmic reticulum-mediated immunity. *Mol. Plant* 11, 1067–1083. <https://doi.org/10.1016/j.molp.2018.05.009>.
26. Broin, M., Cuiné, S., Eymery, F., and Rey, P. (2002). The plastidic 2-cysteine peroxiredoxin is a target for a thioredoxin involved in the protection of the photosynthetic apparatus against oxidative damage. *Plant Cell* 14, 1417–1432. <https://doi.org/10.1105/tpc.001644>.
27. Cain, P., Hall, M., Schröder, W.P., Kieselbach, T., and Robinson, C. (2009). A novel extended family of stromal thioredoxins. *Plant Mol. Biol.* 70, 273–281. <https://doi.org/10.1007/s11003-009-9471-4>.
28. Li, W., Liu, Z., Huang, Y., Zheng, J., Yang, Y., Cao, Y., Ding, L., Meng, Y., and Shan, W. (2024). *Phytophthora infestans* RXLR effector Pi23014 targets host RNA-binding protein NbRBP3a to suppress plant immunity. *Mol. Plant Pathol.* 25, e13416. <https://doi.org/10.1111/mpp.13416>.
29. Mata-Pérez, C., and Spoel, S.H. (2019). Thioredoxin-mediated redox signalling in plant immunity. *Plant Sci.* 279, 27–33. <https://doi.org/10.1016/j.plantsci.2018.05.001>.
30. Holmgren, A. (1979). Thioredoxin catalyzes the reduction of insulin disulfides by dithiothreitol and dihydrolipoamide. *J. Biol. Chem.* 254, 9627–9632. [https://doi.org/10.1016/s0021-9258\(19\)83562-7](https://doi.org/10.1016/s0021-9258(19)83562-7).
31. Knotth, C., and Eulgem, T. (2008). The oomycete response gene *LURP1* is required for defense against *Hyaloperonospora parasitica* in *Arabidopsis thaliana*. *Plant J.* 55, 53–64. <https://doi.org/10.1111/j.1365-313X.2008.03486.x>.
32. Hok, S., Danchin, E.G.J., Allasia, V., Panabières, F., Attard, A., and Keller, H. (2011). An *Arabidopsis* (malectin-like) leucine-rich repeat receptor-like kinase contributes to downy mildew disease. *Plant Cell Environ.* 34, 1944–1957. <https://doi.org/10.1111/j.1365-3040.2011.02390.x>.
33. Liu, Y., Sun, T., Sun, Y., Zhang, Y., Radojičić, A., Ding, Y., Tian, H., Huang, X., Lan, J., Chen, S., et al. (2020). Diverse roles of the salicylic acid receptors NPR1 and NPR3/NPR4 in plant immunity. *Plant Cell* 32, 4002–4016. <https://doi.org/10.1105/tpc.20.00499>.
34. Zeilmaker, T., Ludwig, N.R., Elberse, J., Seidl, M.F., Berke, L., Van Doorn, A., Schuurink, R.C., Snel, B., and Van den Ackerveken, G. (2015). DOWNY MILDEW RESISTANT 6 and DMR6-LIKE OXYGENASE 1 are partially redundant but distinct suppressors of immunity in *Arabidopsis*. *Plant J.* 81, 210–222. <https://doi.org/10.1111/tpj.12719>.
35. Zuccaro, A., and Langen, G. (2020). Breeding for resistance: can we increase crop resistance to pathogens without compromising the ability to accommodate beneficial microbes? *New Phytol.* 227, 279–282.
36. Wawra, S., Fesel, P., Widmer, H., Timm, M., Seibel, J., Leson, L., Kesseler, L., Nostadt, R., Hilbert, M., Langen, G., and Zuccaro, A. (2016). The fungal-specific beta-glucan-binding lectin FGB1 alters cell-wall composition and suppresses glucan-triggered immunity in plants. *Nat. Commun.* 7, 13188. <https://doi.org/10.1038/ncomms13188>.
37. Akum, F.N., Steinbrenner, J., Biedenkopf, D., Imani, J., and Kogel, K.H. (2015). The *Piriformospora indica* effector PIIN_08944 promotes the mutualistic *Sebacinalean* symbiosis. *Front. Plant Sci.* 6, 906. <https://doi.org/10.3389/fpls.2015.00906>.
38. Nostadt, R., Hilbert, M., Nizam, S., Rovenich, H., Wawra, S., Martin, J., Küpper, H., Mijovilovich, A., Ursinus, A., Langen, G., et al. (2020). A secreted fungal histidine- and alanine-rich protein regulates metal ion homeostasis and oxidative stress. *New Phytol.* 227, 1174–1188. <https://doi.org/10.1111/nph.16606>.
39. Yan, Z.-W., Chen, F.-Y., Zhang, X., Cai, W.-J., Chen, C.-Y., Liu, J., Wu, M.-N., Liu, N.-J., Ma, B., Wang, M.-Y., et al. (2023). Endocytosis-mediated entry of a caterpillar effector into plants is countered by Jasmonate. *Nat. Commun.* 14, 6551. <https://doi.org/10.1038/s41467-023-42226-1>.
40. Kale, S.D., Gu, B., Capelluto, D.G.S., Dou, D., Feldman, E., Rumore, A., Arredondo, F.D., Hanlon, R., Fudal, I., Rouxel, T., et al. (2010). External lipid PI3P mediates entry of eukaryotic pathogen effectors into plant and animal host cells. *Cell* 142, 284–295. <https://doi.org/10.1016/j.cell.2010.06.008>.
41. Bi, K., Scalschi, L., Jaiswal, N., Mengiste, T., Fried, R., Sanz, A.B., Arroyo, J., Zhu, W., Msrati, G., and Sharon, A. (2021). The *Botrytis cinerea* Crh1 transglycosylase is a cytoplasmic effector triggering plant cell death and defense response. *Nat. Commun.* 12, 2166. <https://doi.org/10.1038/s41467-021-22436-1>.
42. Stein, E., Molitor, A., Kogel, K.-H., and Waller, F. (2008). Systemic resistance in *Arabidopsis* conferred by the mycorrhizal fungus *Piriformospora indica* requires jasmonic acid signaling and the cytoplasmic function of NPR1. *Plant Cell Physiol.* 49, 1747–1751. <https://doi.org/10.1093/pcp/pcn147>.
43. Vlot, A.C., Sales, J.H., Lenk, M., Bauer, K., Brambilla, A., Sommer, A., Chen, Y., Wenig, M., and Nayem, S. (2021). Systemic propagation of immunity in plants. *New Phytol.* 229, 1234–1250. <https://doi.org/10.1111/nph.16953>.
44. Pieterse, C.M.J., Zamioudis, C., Berendsen, R.L., Weller, D.M., Van Wees, S.C.M., and Bakker, P.A.H.M. (2014). Induced systemic resistance by beneficial microbes. *Annu. Rev. Phytopathol.* 52, 347–375. <https://doi.org/10.1146/annurev-phyto-082712-102340>.
45. Kong, X., Zhang, C., Zheng, H., Sun, M., Zhang, F., Zhang, M., Cui, F., Lv, D., Liu, L., Guo, S., et al. (2020). Antagonistic interaction between auxin and SA signaling pathways regulates bacterial infection through lateral root in *Arabidopsis*. *Cell Rep.* 32, 108060. <https://doi.org/10.1016/j.celrep.2020.108060>.
46. Sun, H., Zhao, W., Liu, H., Su, C., Qian, Y., and Jiao, F. (2020). MaCDSP32 from mulberry enhances resilience post-drought by regulating antioxidant activity and the osmotic content in transgenic tobacco. *Front. Plant Sci.* 11, 419. <https://doi.org/10.3389/fpls.2020.00419>.

47. Geigenberger, P., Thormählen, I., Daloso, D.M., and Fernie, A.R. (2017). The unprecedented versatility of the plant thioredoxin system. *Trends Plant Sci.* 22, 249–262. <https://doi.org/10.1016/j.tplants.2016.12.008>.
48. Sharma, A., Kohli, S.K., Khanna, K., Ramakrishnan, M., Kumar, V., Bhardwaj, R., Brestic, M., Skalicky, M., Landi, M., and Zheng, B. (2023). Salicylic acid: a phenolic molecule with multiple roles in salt-stressed plants. *J. Plant Growth Regul.* 42, 4581–4605. <https://doi.org/10.1007/s00344-022-10902-z>.
49. Pan, Q., Cui, B., Deng, F., Quan, J., Loake, G.J., and Shan, W. (2016). RTP1 encodes a novel endoplasmic reticulum (ER)-localized protein in *Arabidopsis* and negatively regulates resistance against biotrophic pathogens. *New Phytol.* 209, 1641–1654. <https://doi.org/10.1111/nph.13707>.
50. Yin, J., Gu, B., Huang, G., Tian, Y., Quan, J., Lindqvist-Kreuze, H., and Shan, W. (2017). Conserved RXLR effector genes of *Phytophthora infestans* expressed at the early stage of potato infection are suppressive to host defense. *Front. Plant Sci.* 8, 2155. <https://doi.org/10.3389/fpls.2017.02155>.
51. Elnahhal, A.S.M., Li, J., Wang, X., Zhou, C., Wen, G., Wang, J., Lindqvist-Kreuze, H., Meng, Y., and Shan, W. (2020). Identification of natural resistance mediated by recognition of *Phytophthora infestans* effector gene Avr3a(EM) in potato. *Front. Plant Sci.* 11, 919. <https://doi.org/10.3389/fpls.2020.00919>.
52. Yang, Y., Fan, G., Zhao, Y., Wen, Q., Wu, P., Meng, Y., and Shan, W. (2020). Cytidine-to-uridine RNA editing factor NbMORF8 negatively regulates plant immunity to *Phytophthora* pathogens. *Plant Physiol.* 184, 2182–2198. <https://doi.org/10.1104/pp.20.00458>.
53. Du, Y., Chen, X., Guo, Y., Zhang, X., Zhang, H., Li, F., Huang, G., Meng, Y., and Shan, W. (2021). *Phytophthora infestans* RXLR effector PITG20303 targets a potato MKK1 protein to suppress plant immunity. *New Phytol.* 229, 501–515. <https://doi.org/10.1111/nph.16861>.
54. Yin, W., Wang, Y., Chen, T., Lin, Y., and Luo, C. (2018). Functional evaluation of the signal peptides of secreted proteins. *Bio Protoc.* 8, e2839. <https://doi.org/10.21769/BioProtoc.2839>.
55. Chen, H., Zou, Y., Shang, Y., Lin, H., Wang, Y., Cai, R., Tang, X., and Zhou, J.-M. (2008). Firefly luciferase complementation imaging assay for protein-protein interactions in plants. *Plant Physiol.* 146, 368–376. <https://doi.org/10.1104/pp.107.111740>.
56. Kim, D., Paggi, J.M., Park, C., Bennett, C., and Salzberg, S.L. (2019). Graph-based genome alignment and genotyping with HISAT2 and HISAT-genotype. *Nat. Biotechnol.* 37, 907–915. <https://doi.org/10.1038/s41587-019-0201-4>.
57. Tarazona, S., García-Alcalde, F., Dopazo, J., Ferrer, A., and Conesa, A. (2011). Differential expression in RNA-seq: a matter of depth. *Genome Res.* 21, 2213–2223. <https://doi.org/10.1101/gr.124321.111>.
58. Love, M.I., Huber, W., and Anders, S. (2014;15:550). Moderated estimation of fold change and dispersion for RNA-seq data with DESeq2. *Genome Biol.* <https://doi.org/10.1186/s13059-014-0550-8>.
59. Yu, G. (2018). clusterProfiler: An universal enrichment tool for functional and comparative study. Preprint at bioRxiv. <https://doi.org/10.1101/256784>.

STAR★METHODS

KEY RESOURCES TABLE

REAGENT or RESOURCE	SOURCE	IDENTIFIER
Antibodies		
FLAG antibody	ABclonal	Cat# AE005; RRID: AB_2770401
GFP antibody	Abmart	Cat# M20004; RRID: AB_2619674
MYC antibody	ABclonal	Cat# AE010; RRID: AB_2770408
H3 antibody	ABclonal	Cat# A2348; RRID: AB_2631273
Actin antibody	Abmart	Cat# #M20009; RRID: AB_2936239
RuBisCo antibody	Abmart	Cat# M20043
Goat anti-mouse HRP	Abmart	Cat# M21001; RRID: AB_2713950
Goat anti-rabbit HRP	ABclonal	Cat# AS014; RRID: AB_2769854
Bacterial and virus strains		
<i>Escherichia coli</i> DH5 α competent cells	Our laboratory collection	N/A
<i>Escherichia coli</i> BL21 (DE3) competent cells	Our laboratory collection	N/A
<i>Agrobacterium tumefaciens</i> GV3101 electrocompetent cells	Our laboratory collection	N/A
Biological samples		
<i>Phytophthora parasitica</i> strain Pp1121 (with GFP expressed strain Pp016)	Our laboratory collection	N/A
<i>Phytophthora infestans</i> strain Pi88069	Our laboratory collection	N/A
<i>Botrytis cinerea</i> strain Bc001	Our laboratory collection	N/A
<i>Rhizoctonia solani</i> Strain HBZJ-5X	Gifted by Dr. Wu	N/A
<i>Arabidopsis thaliana</i> ecotype Col-0	Our laboratory collection	N/A
<i>Nicotiana benthamiana</i> (wild type)	Our laboratory collection	N/A
<i>Saccharomyces cerevisiae</i> strain AH109	Our laboratory collection	N/A
<i>Saccharomyces cerevisiae</i> strain YTK12	Our laboratory collection	N/A
Chemicals, peptides, and recombinant proteins		
2-Mercaptoethanol	Sigma	M3148
PMSF	Sigma	P7626
Tritonx-100	BioFroxx	1139m100
NaCl	GHTECH	N/A
MgCl ₂	GHTECH	N/A
Sucrose	GHTECH	N/A
MES hydrate	Sigma	M2933
Glycerol	Sigma	G5516
Imidazole	Sigma	I5513
T4 DNA Ligase	Thermo Fisher Scientific	EL0011
FastPfu DNA Polymerase	Transgen	AP221-01
Tris-HCl	VWR Life-Science	22F2956685
EDTA·2Na	VWR Life-Science	3397C237
NP-40	Sigma	492018
PVPP	Sigma	P6755
Protease inhibitor cocktail	Sellechchem	B14001
MG132	Shanghai Yuanye	S42096
HEPES	BioFroxx	1112GR025
2% TTC stain Solution	Coolaber	SL7140-100mL
UltraSYBR Mixture	CWBIO	CW0957S

(Continued on next page)

Continued

REAGENT or RESOURCE	SOURCE	IDENTIFIER
Protein sample loading buffer	Epizyme	LT101S
Western Blot rapid transfer buffer (10X)	Epizyme	PS201S
Western Blot fast stripping buffer	Epizyme	PS107S
Benzonase Nuclease	SMART LIFESCIENCES	SLP00800
Isopropyl β-D-1-thiogalactopyranoside (IPTG)	Sigma	I5502
Lysozyme	Solarbio	L8120
Insulin (bovine pancreas)	Shanghai Yuanye	S12033-100mg
DL-Dithiothreitol (DTT)	Sigma	D0632
PAGE Ruler Protein Ladder	Thermo Fisher Scientific	26617
Anti-GFP Magarose Beads	SMART LIFESCIENCES	SA070001
Yeast Nitrogen Base	Becton	2124288
DO Supplement-His-/Leu-/Trp-/Ura	TAKARA	630425
X-α-gal	Coolaber	CX11922
1/2 MS media	Hopebio	HB8469-12
Plant Agar	Solarbio	A8190
Yeast agar (Bacto™ Agar)	Becton	0063472
Spel	Promega	R6591
Ndel	Promega	R6801
PstI	Promega	R6111
Xhol	Promega	R6161
EcoRI	Promega	R6011
HindIII	Promega	R6041
KpnI	Promega	R6341
SmaI	Promega	R6121
Ncol	Promega	R6513
XbaI	Promega	R6181
NotI	Promega	R6431
Trypan Blue	Sigma	T6416
PEG/LiAC Mixture	Coolaber	YT0006
Carrier DNA	Coolaber	YT0003
Non-fat milk powder	BioFroxx	1172GR500

Critical commercial assays

Plasmid Miniprep Kit	TIANGEN	DP103
TIANquick DNA Purification Kit	TIANGEN	DP203
RNA easy fast plant tissue kit	TIANGEN	DP452
PrimeScript™ RT reagent Kit with gDNA Eraser	TAKARA	#RR047A
ClonExpress II One Step Cloning Kit	Vazyme	C112-01
One-step Color PAGE Gel Rapid Preparation Kit	Epizyme	PG212

Deposited data

RNA sequencing data CK0h R1	This paper	[SRA]: [PRJNA1087523]
RNA sequencing data CK0h R2	This paper	[SRA]: [PRJNA1088257]
RNA sequencing data CK0h R3	This paper	[SRA]: [PRJNA1088286]
RNA sequencing data SIE0h R1	This paper	[SRA]: [PRJNA1088951]
RNA sequencing data SIE0h R2	This paper	[SRA]: [PRJNA1090408]
RNA sequencing data SIE0h R3	This paper	[SRA]: [PRJNA1091039]

Oligonucleotides

Primers for all constructs generations	This study	Table S6
Primers for reference genes	This study	Table S6

(Continued on next page)

Continued

REAGENT or RESOURCE	SOURCE	IDENTIFIER
Recombinant DNA		
pSUC2-PiIN_10643	This study	N/A
pSUC2-Avr1b	This study	N/A
pART27-PKAN-SIE141-GFP	This study	N/A
pART27-PKAN-SIE141CNES-GFP	This study	N/A
pART27-PKAN-AtCDSP32-mCherry	This study	N/A
pART27-PKAN-NbCDSP32-mCherry	This study	N/A
pART27-PKAN-AtUGP1-mCherry	This study	N/A
pART27-PKAN-SIE141-Flag	This study	N/A
pART27-PKAN-SIE141CNES-Flag	This study	N/A
pART27-PKAN-PcAvr3a12-Flag	Fan et al. ²⁵	N/A
pART27-PKAN-AtCDSP32-4myc	This study	N/A
pART27-PKAN-NbCDSP32-4myc	This study	N/A
pART27-PKAN-StCDSP32-4myc	This study	N/A
pART27-PKAN-AtCDSP32 ^{ΔCTP} -4myc	This study	N/A
pART27-PKAN-StCDSP32 ^{ΔCTP} -4myc	This study	N/A
pART27-PKAN-AtCDSP32 ^{ΔSGPS} -4myc	This study	N/A
pART27-PKAN-NbCDSP32CNES-4myc	This study	N/A
pART27-PKAN-NbCDSP32 ^{ΔCTP} CNES-4myc	This study	N/A
pART27-PKAN-ATHM2-4myc	This study	N/A
pART27-PKAN-AtNPR1-4myc	This study	N/A
pART27-PKAN-NbNPR1-4myc	This study	N/A
pART27-PKAN- AtCDSP32-GFP	This study	N/A
pART27-PKAN- NbCDSP32-GFP	This study	N/A
pART27-PKAN- StCDSP32-GFP	This study	N/A
pMDC32-AtNPR1-Flag	This study	N/A
pKANNIBEL-RNAi-AtCDSP32	This study	N/A
pGBKT7-SIE141	This study	N/A
pGADT7-NbCDSP32	This study	N/A
pGADT7-PSBR	This study	N/A
pGADT7-NbCDSP32	This study	N/A
pGADT7-AtCDSP32 ^{ΔCTP}	This study	N/A
pGADT7-NbCDSP32 ^{ΔCTP}	This study	N/A
pGADT7-ATF2	This study	N/A
Cluc-SIE141	This study	N/A
Nluc-NbCDSP32	This study	N/A
Cluc-AtCDSP32	This study	N/A
Cluc-NbCDSP32	This study	N/A
Nluc-AtNPR1	This study	N/A
Nluc-NbNPR1	This study	N/A
TRV2-NbCDSP32	This study	N/A
pDEST-VYNE(R)GW-SIE141	This study	N/A
pDEST-VYNE(R)GW-Pi23014	Li et al. ²⁸	N/A
pDEST-GWVYCE-NbCDSP32	This study	N/A
pET32a-SIE141	This study	N/A
pET32a-AtCDSP32	This study	N/A
pET32a-NbCDSP32	This study	N/A
pET32a-StCDSP32	This study	N/A
pET32a-ATH5	This study	N/A

(Continued on next page)

Continued

REAGENT or RESOURCE	SOURCE	IDENTIFIER
Software and algorithms		
ImageJ (1.49v)	https://imagej.nih.gov/ij/	N/A
GraphPad Prism 8.0	Prism	N/A
Mega X	https://www.megasoftware.net/dload_win_gui	N/A
iTOL	https://itol.embl.de/	N/A
NLStradamus	http://www.moseslab.csb.utoronto.ca/NLStradamus/	N/A
SignalP	https://services.healthtech.dtu.dk/services/SignalP-6.0/	N/A
Clustal Omega	https://www.ebi.ac.uk/jdispatcher/msa/clustalo	N/A
Other		
NanoDrop™ One	Thermo Fisher Scientific	N/A
Eporator Electroporator	Bio-Rad	N/A
Plantview 100	BLT Photon Technology	N/A
Ultra-High Resolution LC-MS	Thermo Fisher Scientific	Fusion Lumos
LC-MS-MS QTRAP5500	AB Sciex	N/A
Lecia TCS SP8 MP Multiphoton Microscope	LECIA	N/A
LightCycler® 480 Instrument	Roche	N/A
Ultrasonic Homogenizer	SCIENTZ	N/A
Varioskan LUX	Thermo Fisher Scientific	N/A
ChemiDocMP	Bio-Rad	N/A
Olympus FV3000	Olympus	N/A

RESOURCE AVAILABILITY

Lead contact

Further information and requests for resources and reagents should be directed and will be fulfilled by the lead contact, Weixing Shan (wxshan@nwafu.edu.cn).

Materials availability

Unique materials generated in this study are available from the lead contact without restriction.

Data and code availability

- All data reported in this paper will be shared by the lead contact upon request. The RNA-seq raw data are available in the SRA database at NCBI. Detailed BioProject accession numbers are listed in the [key resources table](#).
- This paper does not report original code.
- Any additional information required to reanalyze the data reported in this work paper is available from the lead contact upon request.

EXPERIMENTAL MODEL AND STUDY PARTICIPANT DETAILS

Plant growth conditions and surface sterilization steps

All plants generated for this study were created on the *A. thaliana* ecotype Col-0 background. Plants were grown at 23°C under a 13/11 h light/dark cycle in growth chambers. For in vitro seedlings, *A. thaliana* seeds were surface sterilized with 75% ethanol for 30 s, rinsed with sterilized MiliQ water once, subsequently sterilized with 1% NaClO for 8 min, and rinsed with sterilized MiliQ water for four times, dried on sterilized paper before being planted on ½ MS media (with sucrose and agar), vernalized in 4°C in the dark for 2 d and then moved into the growth chamber.

Bacteria, yeasts, *Phytophthora* and fungal pathogens, and their growth conditions

Transient expression assays, *A. thaliana* transformations, and VIGS assays were performed with *Agrobacterium tumefaciens* GV3101.

Saccharomyces cerevisiae strains AH109 and YTK12 were used for yeast transformations (and mating) and signal peptide secretion experiments. All yeast strains were cultured at 30°C on 2× YPDA media.

Pathogen inoculation assays used *P. parasitica* strain Pp1121 (with stable GFP expression) and *P. infestans* strain Pi88069. *P. parasitica* was cultured in carrot juice (CA) medium at 23°C⁴⁹ in dark and *P. infestans* was cultured in rye sucrose agar (RSA) medium at 16°C⁵⁰ in dark. *Botrytis cinerea* (strain Bc001) was cultured on potato dextrose agar (PDA) at 16°C in dark and the conidia was collected for infection with PDB (Potato dextrose broth) until black sclerotia grown. *Rhizoctonia solani* (strain HBZJ-5X) was cultured on PDA at 23°C in dark.

METHOD DETAILS

Plasmid construction

The open reading frame of *PIIN_10643* (without the repeat domain at the C-terminus and excluding the signal peptide) (*SIE141*) was inserted into pART27 at the *Xhol*-*EcoRI* sites¹⁴ with a Flag and a GFP tag. The target genes *AtCDSP32*, *NbCDSP32*, and *StCDSP32* were amplified from *A. thaliana*, *N. benthamiana*, and *S. tuberosum*, respectively. Each gene was then fused with a 4×Myc tag and inserted into pART27 at the *Xhol*-*HindIII* sites. The resulting plant expression vectors were used for *A. thaliana* transformant preparation or co-IP or transient expression assays. The new GATEWAY vectors were used for BiFC assays. For Y2H assays, *SIE141* was cloned into pGKKT7 at the *NdeI*-*PstI* sites. Target genes were amplified from *N. benthamiana* cDNA and cloned into pGADT7 at the *NdeI*-*Xhol* sites. To generate VIGS constructs, a 300-bp fragment of *NbCDSP32* was amplified from *N. benthamiana* cDNA and cloned into the binary vector pTRV2 at the *KpnI*-*SmaI* sites. TRV2::GFP was constructed as a control. To generate the vectors used for signal peptide functional analyses, *PIIN_10643* signal peptides were synthesized and inserted into the *EcoRI*-*Xhol* restriction sites of pSUC2²² using a ClonExpress II One Step Cloning Kit (Vazyme). A 300-bp fragment was selected from *AtCDSP32* for RNA silencing to minimize off-target effects. The fragment was amplified and cloned into the pKannibal vector between the *Xhol*-*EcoRI* sites in sense orientation and between the *HindIII*-*XbaI* sites in antisense orientation. Finally, the construct was subcloned into the binary vector pART27 at the *NotI* site. Prokaryotic expression vectors were generated using a pET32a vector with an N-terminal His tag. The coding sequences of *SIE141*, *AtCDSP32*, *NbCDSP32*, *StCDSP32* and *ATH5* were inserted into the vector at the *Ncol*-*Xhol* sites. All constructs were sequenced by Tsingke (Beijing, China). Primers used for plasmid construction are shown in Table S6.

Pathogen infection assays

Maintenance and zoospore production of *P. parasitica* strain Pp016 and the stable GFP-expressing transformant strain 1121 were conducted as previously described.¹⁵ Fully-covered *P. parasitica* mycelia agar plates (4 d) were cut into pieces and cultured with liquid CA media at 23°C in the dark for 4 d. Mycelia agar pieces were washed 4 times with sterilized water and then cultured in a salt solution¹⁵ for 7 d. To stimulate zoospore release, mycelia agar pieces in salt solution were washed for 4 times and held in sterilized water at 4°C for 30 min, followed by 23°C for 30–60 min, until the zoospores released.

For root inoculation assays, *A. thaliana* seedlings were grown on ½ MS media. The roots were dipped in *P. parasitica* strain 1121 zoospores (10⁵ spores/ml), then the seedling survival rates were calculated at 10 dpi.⁴⁹ Samples for quantification of pathogen biomass were collected from *P. parasitica*-infected *A. thaliana* seedlings. For each replicate, at least 15 infected seedlings were collected. For detached leaf assays, fully expanded apical *A. thaliana* leaves were wounded with a toothpick, then 10 µl of zoospore suspension (200 zoospores/µl) was applied directly to each wound site.¹⁵ Disease symptoms were scored using a five-rank system as described by Yang et al.¹³ For *N. benthamiana* assays, 20 µl of 1121 zoospore suspension was directly applied to the abaxial side of detached leaves. Leaves were stained with trypan blue at 48 h post-inoculation (hpi) to observe lesion diameters.

A suspension of *P. infestans* strain Pi88069 zoospores was prepared as previously described.⁵¹ Pre-cold sterilized water was added to full-grown mycelia of *P. infestans*, and mycelia was scrubbed with sterilized pipette tips, followed by 4°C cold treatment for 1 h until the zoospore release. 20-µl droplets of the suspension (10⁵ zoospores/ml) were applied to detached *N. benthamiana* leaves. Leaves were stained with trypan blue at 4–5 dpi, then lesion diameters were observed. *P. parasitica* and *P. infestans* biomass were quantified in infected *A. thaliana* and *N. benthamiana* leaves, respectively, using previously reported methods.^{15,52} Three infected detached leaves of individual *A. thaliana* line or agrobacteria-infiltrated *N. benthamiana* were collected as 3 individual bio-replicates, followed by DNA extractions. The DNA concentrations for all groups were adjusted to a similar level for qPCR test.

Transient expression and VIGS assays in *N. benthamiana*

Agrobacterium transient expression assays were carried out in 4-week-old *N. benthamiana* as previously described.¹⁴ VIGS assays were performed using a previously described method.⁵³ The *NbCDSP32* fragment was cloned into TRV2, with a TRV2 vector containing *GFP* serving as a control. The silencing effect was monitored in phytoene desaturase (PDS)-silenced plants as an indicator for the properly silenced leaves. The lower leaves of six-leaf stage *N. benthamiana* were infiltrated with a mixture of Agrobacterium cultures containing TRV1 and TRV2 in equal proportions (final OD₆₀₀ = 0.3). VIGS plants were analyzed 3–5 weeks after infiltration.

Yeast two-hybrid (Y2H) assay

The Matchmaker Two-Hybrid System 3 protocol (Clontech) was used for all Y2H assays. The effector gene *SIE141* was inserted into the pGKKT7 vector as the bait. The coding sequences corresponding to putative interacting proteins were cloned into the pGADT7

vector as prey. The pGBKT7-SIE141 and pGADT7 vectors, each containing a selection gene, were co-transformed into the yeast strain AH109. Transformations were verified by plating on SD-/Trp-Leu media (DDO). Depending on the experiment, interactions were confirmed based on growth on SD-/Trp-Leu-His media (TDO) containing 2.5 mM 3-amino-1,2,4-triazole (3AT); gain of α -galactosidase activity (X-a-gal).

Bimolecular fluorescence complementation (BiFC) assay

BiFC assays were performed as previously described.¹⁴ The binary vectors pDEST-VYNE(R)GW and pDEST-GWVYCE were used. Individual Agrobacterium cultures were transformed with each vector, then the appropriate pairs of *Agrobacterium* cultures were transiently co-infiltrated into *N. benthamiana* leaves. Fluorescence was observed at 2 days post-infiltration with confocal microscope.

Co-immunoprecipitation assay (co-IP) and western blot assays

Proteins were extracted from *N. benthamiana* leaves expressing co-IP constructs at 2 days post-infiltration. Extractions were conducted with RIPA lysis buffer (25 mM Tris-HCl, pH 7.5, 150 mM NaCl, 1 mM EDTA, and 0.5% NP-40) with 2% (w/v) polyvinylpoly-pyrrolidone (PVPP), 1 mM dithiothreitol (DTT), and 10 μ l 100X protease inhibitor cocktail (Sellechchem). Total protein samples were incubated at 4°C for 4 h with 20 μ l Anti-GFP Magarose Beads. For each sample, beads were pre-washed three times with IP buffer (10 mM Tris-HCl, pH 7.5, 150 mM NaCl, and 0.5 mM EDTA) at 4°C for 1 min. The resuspended GFP-Trap beads were mixed with 6 \times loading buffer and boiled for 10 min at 95°C to dissociate the immunocomplexes prior to sodium dodecyl sulfate (SDS)-polyacrylamide gel electrophoresis (PAGE). SDS-PAGE was performed using a Fast Preparation Kit. Antibodies are listed in the [key resources table](#).

Functional evaluation of PIIN_10643 signal peptide sequences

The sequence encoding the predicted signal peptide (residues 1–18 at the N-terminus of PIIN_10643) was inserted into the pSUC2 vector at the EcoRI-Xhol sites. After verification with sequencing, the resulting pSUC2 construct was transformed into yeast YTK12 competent cells as previously described.²² All transformants were grown on selective complete minimal medium lacking tryptophan (CMD-W) agar plates, then cultured in 3 ml of CMD-W broth at 30°C with shaking for 36 h. Further functional evaluation was performed following a previously published protocol.⁵⁴ Yeast cells were harvested via centrifugation (1000 \times g for 10 min) and washed twice with sterilized Milli Q water. Subsequently, cells were resuspended in 750 μ l Milli Q water with 250 μ l of 10 mM NaOAc (pH 4.7) and 500 μ l of 10% sucrose (w/v). After incubation in a water bath at 37°C for 10 min, 900 μ l of 0.1% TTC solution was added and samples were incubated at room temperature for 5 min. Those YTK12 strains carrying a functional signal peptide can secrete invertase and reduce TTC to the insoluble red compound 1,3,5-Triphenylformazan (TPF) and color the solution.

Recombinant protein purification

E. coli, strain BL21 (DE3) carrying pET32a-SIE141, pET32a-AtCDSP32, pET32a-NbCDSP32, pET32a-StCDSP32, or pET32a-ATH5 was grown overnight in 5 ml lysogeny broth (LB) with ampicillin at 37°C. This overnight culture was then transferred into 1 L of LB with ampicillin and grown to an OD₆₀₀ between 0.6 and 0.8. Isopropyl β -d-1-thiogalactopyranoside (IPTG) was then added to the culture to a final concentration of 0.8 μ M prior to incubation at 37°C for 4 h. Bacteria were collected by centrifugation at 6000 \times g for 10 min, then resuspended in 5 mM Tris buffer, 400 μ l 100mM PMSF (Phenylmethanesulfonyl fluoride), 0.04 g lysozyme, and 2.5 μ l DNase I to final 40 ml system. The lysozyme-treated, resuspended bacteria were disrupted with Ultrasonic Homogenizer for 30 min (30 W, 20 kHz, interval 3 seconds), then centrifuged at 12000 \times g for 30 min. The supernatant was purified with a His Sepharose affinity column and eluted with 250 mM imidazole. The eluate was dialyzed at 4°C against 1 M imidazole overnight. The concentrations of the recombinant protein solutions were calculated using the Bradford method. Protein expression levels were determined with 10% SDS-PAGE followed by Coomassie brilliant blue staining.

Thioredoxin activity assay

TRX-h activity was evaluated as previously described.³⁰ Each reaction system was contained in a single 300- μ l well of a clear enzyme-linked immunosorbent assay (ELISA) plate. Each 120- μ l reaction mixture contained 63 mM potassium phosphate buffer (pH 7.0), 100 mM DTT, 2 mM EDTA, and 1 mg/ml bovine insulin. Thioredoxins were present at a range of concentrations, with control samples excluding thioredoxins. Enzymatic reactions were initiated by adding 0.33 mM DTT. Turbidity was measured at 650 nm for at least 60 min. A specific concentration of TRX was selected for further analysis. Varying concentrations of SIE141 were co-incubated with the selected concentration of thioredoxin, then added to the reaction mixture. A PiAvr3a mutant (SAM5 or SAM6) was used as a negative control for enzyme activity in co-incubation of the effector and thioredoxins. Turbidity was monitored at 650 nm for at least 60 min.

Real-time quantitative PCR (qRT-PCR) and quantitative reverse transcription PCR (RT-qPCR)

RNA extractions were performed with the Total RNA Extraction Kit (TIANGEN). cDNA was synthesized from the resulting RNA using PrimeScript™ RT reagent Kit with gDNA Eraser (TAKARA) for qPCR. qPCR was performed on a LightCycler® 480 Instrument (Roche

Life Science) with the UltraSYBR Mix (CWBIO). For gene expression analyses, differences in transcript levels between treatments were calculated according to plant species-specific reference genes following this formula:

$$\text{Transcript level (Fold induction)} = \frac{E_{\text{target}}^{\Delta Ct - \text{target}(\text{control} - \text{sample})}}{E_{\text{reference}}^{\Delta Ct - \text{reference}(\text{control} - \text{sample})}}$$

E_{target} : Primer efficiency of target genes (assumed as 2); $E_{\text{reference}}$: Primer efficiency of housekeeping genes (assumed as 2); Ct: Ct cycle detected.

The plant species-specific reference genes *AtUBC9* (AT4G27960) and *NbEF1 α* (Niben101Scf04639g06007) were employed for *A. thaliana* and *N. benthamiana*, respectively. Primers are shown in [Table S6](#).

Reduction of NPR1 oligomers to monomers by thioredoxins

Leaf tissue samples (2 g each) from uninduced 35S::NPR1-FLAG plants were homogenized with 1.5 ml of 10 mM HEPES pH = 7.7, 40 μ M MG132 (Z-Leu-Leu-Leu-al) and 10 μ l 100 \times protease inhibitor cocktail (Sellechchem). The supernatant was recovered by centrifugation at 4°C and 14,000 \times g for 20 min, then dialyzed against 10 mM HEPES (pH 7.7) for 1 h. The dialyzed extraction solution was mixed with 40 μ M MG132 and protease inhibitor cocktail. Samples (90 μ l each) were incubated with 0.33 mM DTT and 50 μ M ATH5/AtCDSP32/NbCDSP32/StCDSP32 recombinant protein for 30 min; samples excluding CDSP32 were used as the positive control. Immunoblots were then performed with 7.5% SDS-PAGE to measure NPR1-FLAG.

Confocal microscopy

Cells were visualized with Olympus FV3000 or Leica confocal microscope for BiFC and protein subcellular localization assays. The excitation wavelengths used for YFP and GFP were 514 and 488 nm, respectively, and the emissions of both were detected between 500 and 540 nm. mCherry was excited at 559 nm and specific emissions between 600 and 680 nm were collected. Image processing and figure generation were conducted with Olympus Fluoview or Leica TCS SP8 MP Multiphoton Microscope.

SA measurements with HPLC-MS/MS

For SA measurements, *A. thaliana* seedlings were collected and weighed. Each biological replicate per genotype comprised ~0.3–0.4 g of tissue (roots or leaves), which was ground to powder in liquid nitrogen, then combined with extraction reagent (1:4 methanol: isopropyl alcohol). Samples were vortexed for 5 min and stored at 4°C overnight. After centrifugation at 12000 \times g for 10 min, the supernatant was removed with a 1-ml syringe and filtered through a nylon membrane (0.22- μ m pore size). For each sample, free SA was measured in 500 μ l of the filtrated mixture with HPLC-MS (QTRAP5500). Retention time, 6.68 min, Q1 = 136.5, Q3 = 93.3, DP = -50, CE = -25.

Luciferase assay

The firefly Luciferase assays were performed according to the protocol described by Chen et al.⁵⁵ *AtNPR1*, *NbNPR1* and *NbCDSP32* genes were amplified and cloned into the vector NLuc at the *Kpn*I-SmaI sites. *SIE141*, *AtCDSP32* and *NbCDSP32* were amplified and cloned into the vector Cluc at the *Kpn*I-SmaI sites. Successfully generated constructs were transferred into Agrobacteria respectively. Agrobacterial cell suspensions in MES solution were adjusted to OD₆₀₀ of 0.3. Agrobacterial cell suspensions carrying different gene constructs were mixed before infiltration into *N. benthamiana*. Luciferase activity was monitored and quantified with Plantview 100 (BLT company).

RNA sequencing and transcriptome analysis

The 10-day-old Col-0, OESIE141#1 and OESIE141#3 *A. thaliana* lines were collected for RNA extraction and subsequent transcriptome analysis. For each *A. thaliana* line, 3 biological repeats with at least 0.2 g samples were prepared. The RNA sequencing was conducted with BGI genomics company (Shenzhen, China). Original transcriptome data including Accessions, count reads, p-value, gene ratios of all identified genes were given by the company.

For transcriptome analysis, clean reads of 3 bio-replicates from each line were mapped to the Arabidopsis genome (TAIR10, www.arabidopsis.org) used HISAT2,⁵⁶ after screening and trimming. The number of raw reads and mapped reads to the reference genome is listed in [Table S4](#). Cufflinks methods were used for determination of expression values.⁵⁷ DEseq2⁵⁸ was used to find different expression genes (DEGs). Genes with estimated absolute fold changes ≥ 2 and p-value adjustment (*p.adj*) ≤ 0.05 were identified as reliable DEGs. R (<https://www.r-project.org/>) was used for visualization. ClusterProfiler was used to do gene GO ontology analysis for the DEGs, the SAR pathway genes were screened for next step analysis⁵⁹ ([Table S5](#)). The RNA-seq raw data are available in SRA database from NCBI, with BioProject accession numbers RJNA1087523, PRJNA1088257, PRJNA1088286, PRJNA1088951, PRJNA1090408 and PRJNA1091039.

Salt stress treatment and analysis

Various *A. thaliana* lines were planted directly on 1/2 MS+150 mM NaCl media plates and 1/2 MS media plates. 36 seeds of each *A. thaliana* line were planted for individual bio-repeats. Plates with seeds were put in a growth chamber at 23°C under a 13 h: 11 h, light: dark cycle for 5 days and the germination rate was observed for each line. Ten days after germination, fresh weight of individual seedlings was measured. Data were calculated with one-way ANOVA at *P* < 0.05.

For salt treatment in soil experiments, 4-week-old *A. thaliana* seedlings were irrigated with 50 ml 250 mM NaCl. The mock group was irrigated with 50 ml miliQ water. Leaves from the same leaf arrangement were detached and photographed at 7 days post treatment followed by the measurements of leaf area with imageJ. Fresh weight of leaves (2 individual leaves were collected as one replicate) were measured, ground with liquid nitrogen into fine powder, and suspended in 1 ml of 95% ethanol at 4°C overnight. Absorbance at OD₆₆₅ (A665) and OD₆₄₉ (A649) were measured and recorded. Total chlorophyll concentration (mg/L) was calculated as: 13.95A665-6.88A649 + 24.96A649-7.32A665. Ratio of chlorophyll a/ chlorophyll b was calculated as: (13.95A665-6.88A649)/(24.96A649-7.32A665). Data were calculated with one-way ANOVA at $P < 0.05$.

Cytoplasm and nuclear fraction separation and protein extraction

N. benthamiana leaves expressing AtCDSP32-GFP, NbCDSP32-GFP and StCDSP32-GFP together with either SIE141-FLAG or PcAvr3a12-FLAG were ground with liquid nitrogen. Add 10 ml precooled extraction buffer I (0.4 M sucrose, 10 mM pH=8.0 Tris-HCl, 10 mM MgCl₂, 5 mM β-ME (2-Mercaptoethanol), 0.1 mM PMSF, Triptonx-100 1% with 1× protease inhibitor cocktail), vortex followed by spinning for 30 min with rotary mixer. The extracted liquid was filtrated with gauze, followed by centrifugation at 4000 × g, 20 min, 4°C. The supernatant was collected and 1 ml extraction buffer II (0.25 M sucrose, 10 mM pH=8.0 Tris-HCl, 10 mM MgCl₂, 5 mM β-ME, 0.1 mM PMSF, Triptonx-100 1% with 1× protease inhibitor cocktail) added. Supernatant was removed after centrifugation at 12000 × g, 10 min, 4°C and 600 μl extraction buffer III (1.7 M sucrose, 10 mM pH=8.0 Tris-HCl, 2 mM MgCl₂, 5 mM β-ME, 0.1 mM PMSF, Triptonx-100 0.15% with 1× protease inhibitor cocktail) were added to resuspend the pellet. Carefully, the 600 μl suspension was added to 600 μl new extraction buffer III and centrifuged for 60 min, 14000 × g, 4°C. The supernatant was removed and resuspended with 700 μl Nuclei Lysis buffer (50 mM pH=8.0 Tris-HCl, 10 mM EDTA, 1% SDS, 2 mM PMSF, with 1× protease inhibitor cocktail) to get the proteins in nuclear fraction.

The supernatant after centrifugation was collected. Protein was extracted from 4 ml of the supernatant with 1 ml RIPA lysis buffer (mentioned previously in co-IP and western blot assays), vortexed and left on ice for 10 min. 5 ml supernatant were transferred and 20 ml precooled acetone was added. precipitated at -20°C overnight and then centrifuged at 4°C, 12000 × g for 15 min. The pellet was dissolved with 1 ml HEPEs buffer (10 mM, pH = 7.7) to get proteins in the cytoplasmic fraction.

Phylogenetic tree construction for orthologs of CDSP32

The amino sequences of CDSP32 of different plant species were from Uniport database (Table S2). Alignment of these aa sequences was conducted with Clustal Omega. The phylogenetic tree was constructed with Mega X using maximum likelihood method. The tree was drawn by iTOL (<https://itol.embl.de/>).

QUANTIFICATION AND STATISTICAL ANALYSIS

Image processing and data analysis

Confocal microscopy images were processed with Leica Application Suite X (LAS X) or Olympus Fluoview and Fiji (imageJ version 1.49v). To quantify protein co-localization, the TIF confocal graphs were opened in imageJ, the channels were split based on original colors, and the fluorescence intensity of each individual color channel was from lines drawn on the specific sites. The resulting plot file data for the gray value was prepared as a single graph in Prism GraphPad.

Statistical analysis

Raw data from all pathogen infection experiments (lesion diameters, survival rates, percentage of disease degree), from salt stress assays (fresh weights, germination rates, total chlorophyll contents, ratio of chlorophyll a/b and leaf area), from qPCR assays (relative transcript levels and pathogen biomass), and from cell counts with nuclear-localized CDSP32 were processed with MS Excel. GraphPad Prism 8.0 was used to graph normal bar charts, stacked bar and line charts as well as statistical analysis. One-way analysis of variance (ANOVA) with post hoc analysis of Tukey HSD test, Fisher's LSD test, Brown-Forsythe or Welch test, was used to study the relationship between different treatments, as specifically described in figure legends. Lowercase letters in bar charts indicate statistical significance tested between multiple groups by one-way ANOVA at $P < 0.05$. Student t-test analysis was conducted in MS excel, either a non-paired t-test or a paired t-test was described in the figure legends. For the data shown with stacked bar charts (percentage of disease degree and quantification of the frequency of nuclear CDSP32 relocation), nonparametric statistical analysis (Rank sum test) was conducted in GraphPad Prism 8.0 with Mann Whitney Wilcoxon test. "n" usually represents the number of seedlings tested or the number of bio-repeats tested. For survival rate tests, 7~8 *A. thaliana* seedlings per plate of ½ MS media were evaluated for *P. parasitica* or *R. solani* infection, and the obtained survival rate data treated as a single replicate as one "n". For biomass tests, 3 independent repeats with more than 15 seedlings tested, n represents bio-repeats. Normal bar charts indicate data of the mean with SEM (standard error of mean).